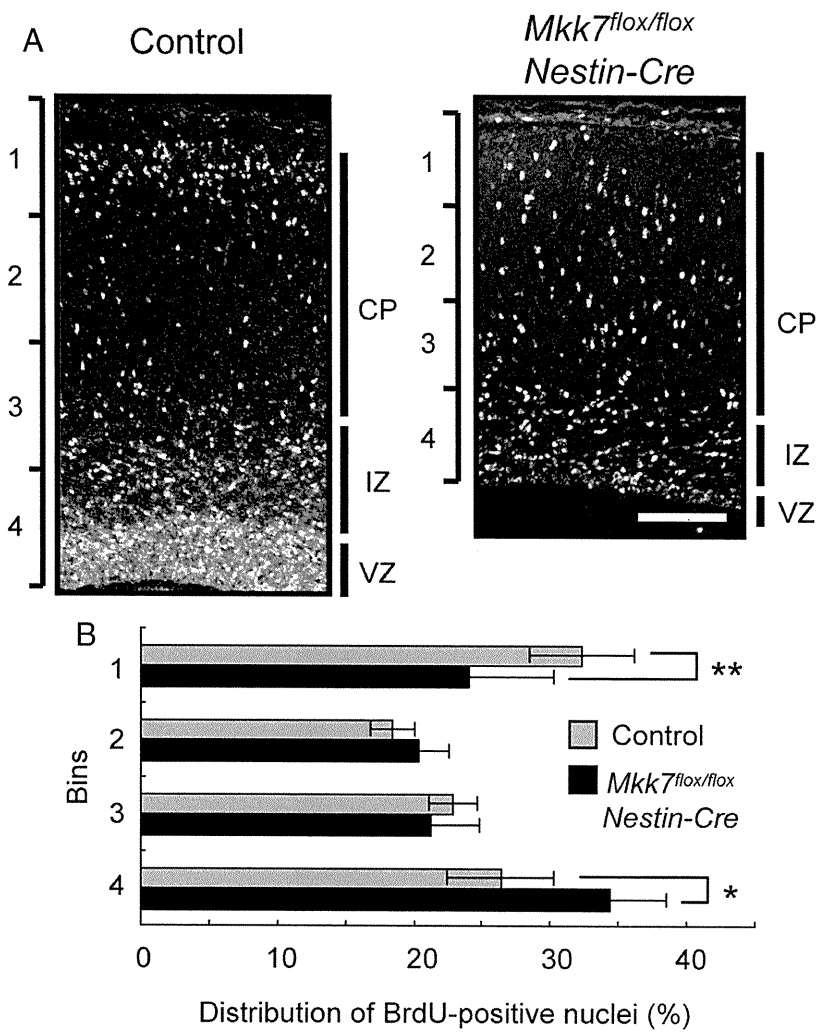

Figure 6. MKK7 deletion delays neuronal radial migration in the cortex. ***A***, Control and *Mkk7*$^{flox/flox}$ *Nestin-Cre* embryos were labeled *in utero* with BrdU at E15.5 and coronal sections were prepared at E18.5 and analyzed by immunostaining with anti-BrdU antibody. White, BrdU. Scale bar, 100 μm. CP, cortical plate; IZ, intermediate zone. ***B***, Distribution of BrdU-positive nuclei. The immunostained cortices in ***A*** were divided into four equal bins from the pial side to the ventricular side. The percentage of the total number of immunostained nuclei in a particular bin was determined and the results plotted in a histogram. Data shown are the mean ± SD ($n = 6$). $^{*}p < 0.05$; $^{**}p < 0.01$.

embedded in Epon812, and thin sections (70–80 nm) were cut and stained with uranyl acetate and lead citrate for observation under a Jeol-1010 electron microscope (Jeol) at 80 kV.

Plasmids. All genes were expressed under the control of the CAG promoter. pCAG-NLS-Cre and pCAG-floxed-polyA-EGFP were kindly provided by Dr. Fumio Matsuzaki (RIKEN-CDB, Japan). pCAG-EGFP-MKK7, pCAG-EGFP-MKK4, pCAG-MKK7-JNK, pCAG-c-Jun-IRES-EGFP, and pCAG-EGFP-JBD were constructed in the Nishina laboratory using standard protocols. Plasmids were purified using the Endofree Plasmid Maxi kit (Qiagen).

Statistical analysis. Data were analyzed using the paired Student's *t* test for two-tailed distributions. Significance levels were as follows: $^{*}p < 0.05$, $^{**}p < 0.01$, $^{***}p < 0.001$, $^{****}p < 0.0001$.

Results

Mkk7$^{flox/flox}$ *Nestin-Cre* mice die at P0 without breathing

Because MKK7 total knock-out mice are embryonic lethal, it has not been possible to examine MKK7 functions in the brain. To confirm that MKK7-JNK signaling occurs during normal brain development, we established a time course of JNK phosphorylation and MKK7 activity in wild-type (WT) mouse brain. Extracts of brains of embryos from E12.5 to adult were prepared and immunoblotted to detect total and activated JNK. MKK7 activity was measured by *in vitro* kinase assay. We found that JNK and MKK7 were highly activated from the E16.5 to the adult stages (Fig. 1*A*,*B*, and data not shown). These data establish that MKK7-JNK signaling occurs during normal brain development.

To investigate the role of this MKK7-JNK signaling *in vivo*, we made a mutant mouse carrying a *mkk7 flox* allele (Fig. 1*C*), and crossed it with a transgenic mouse line that expresses Cre under the control of the *nestin* promoter (Imai et al., 2006). We confirmed the deletion of *mkk7* in *Mkk7*$^{flox/flox}$ *Nestin-Cre* brain at E16.5 by Southern blotting (Fig. 1*D*). As expected, levels of MKK7 and phosphorylated JNK proteins were markedly reduced in the brains of these mice, but, unexpectedly, phospho-MKK4 was upregulated (Fig. 1*E*). These results suggest that, in the absence of one JNK regulator (MKK7), the activation of another JNK regulator (MKK4) may increase in compensation.

To investigate whether MKK7 was important for postnatal viability, we intercrossed *Mkk7*$^{flox/+}$ *Nestin-Cre* and *Mkk7*$^{flox/flox}$ mice and determined the genotypes of embryos and postnatal pups. Surprisingly, although *Mkk7*$^{flox/flox}$ *Nestin-Cre* mice appeared normal through all embryonic stages, no mutants were detected on P1 (Table 1). To determine whether *Mkk7*$^{flox/flox}$ *Nestin-Cre* mice died at birth, we performed caesarean sections and found that *Mkk7*$^{flox/flox}$ *Nestin-Cre* mice were indistinguishable from controls at E18.5. However, all but one *Mkk7*$^{flox/flox}$ *Nestin-Cre* mouse died immediately without breathing after caesarean section (Fig. 1*F*). MKK7 is therefore vital for postnatal survival.

Abnormal brain development in *Mkk7*$^{flox/flox}$ *Nestin-Cre* mice

The death of *Mkk7*$^{flox/flox}$ *Nestin-Cre* mutants at birth suggested that there might be defects in the brains of these animals. To assess brain histology, sections of various brain structures were prepared from control (*Mkk7*$^{flox/+}$, *Mkk7*$^{flox/flox}$, and *Mkk7*$^{flox/+}$ *Nestin-Cre*) and *Mkk7*$^{flox/flox}$ *Nestin-Cre* mice at E18.5 and stained with cresyl violet. Although *Mkk7*$^{flox/flox}$ *Nestin-Cre* whole brain was grossly indistinguishable from control littermate whole brain (Fig. 2*A*), histological analysis showed that *Mkk7*$^{flox/flox}$ *Nestin-Cre* brain had larger ventricles and a reduced striatum compared to control brain (Fig. 2*B*). In addition, whereas the corpus callosum (CC) and the anterior commissure (AC) were clearly formed in control E18.5 brain, these commissural axon tracts were barely detectable in E18.5 *Mkk7*$^{flox/flox}$ *Nestin-Cre* brain (Fig. 2*B*,*C*). Moreover, although there was no defect in the mutant hippocampal commissure (data not shown), the internal capsule (IC), which consists of axonal fibers connecting the cerebral cortex and subcortical brain regions, was reduced in size in *Mkk7*$^{flox/flox}$

Nestin-Cre brain (Fig. 2*D*). These data indicate that MKK7 regulates the formation of axon tracts during brain development.

To further examine the effect of MKK7 deletion on axon tracts, we used electron microscopy to look for ultrastructural alterations in *Mkk7*$^{flox/flox}$ *Nestin-Cre* brain. We found that abnormally electron-dense axons were present in *Mkk7*$^{flox/flox}$ *Nestin-Cre* cortex and striatum (Fig. 3*A*,*B*), and that these structures contained an accumulation of intermediate filaments (Fig. 3*A*, inset). In addition, autophagic vacuoles and swollen mitochondria were detected in the striatum, cortex, and brainstem of *Mkk7*$^{flox/flox}$ *Nestin-Cre* brain (Fig. 3*B* and data not shown). Thus, MKK7-mediated regulation of JNK may be important for suppressing autophagy and controlling the distribution of intermediate filaments in the developing brain.

Impaired axon formation

Our histological analyses led us to hypothesize that MKK7-JNK signaling might normally be activated in the axons of WT developing brain. As expected, phospho-JNK coimmunostained with L1, which is a cell adhesion molecule expressed on axons, in control brain but was reduced in *Mkk7*$^{flox/flox}$ *Nestin-Cre* brain (Fig. 4*A*). We then performed a more detailed analysis by immunostaining to detect both L1 and transient axonal glycoprotein-1 (TAG-1), which is expressed in corticofugal axons (Wolfer et al., 1994; Denaxa et al., 2001). In *Mkk7*$^{flox/flox}$ *Nestin-Cre* brain at E18.5, we found that numbers of L1-positive as well as TAG-1-positive axons were decreased in the cortex and CC compared to controls (Fig. 4*B*,*C*). These results indicate that MKK7 has a particularly important role in the formation of TAG-1-positive axons.

Because previous reports implicated JNK in regulating apoptosis during brain development (Kuan et al., 1999; Sabapathy et al., 1999), we examined whether apoptosis was altered in *Mkk7*$^{flox/flox}$ *Nestin-Cre* brain. Immunostaining with antibody specific for cleaved caspase-3 revealed that, like control brain, there were few apoptotic cells in the *Mkk7*$^{flox/flox}$ *Nestin-Cre* cortex (Fig. 5*A*). Apoptotic cells were also rare in the striatum of both *Mkk7*$^{flox/flox}$ *Nestin-Cre* and control brains (data not shown). A few apoptotic cells were observed surrounding the mutant CC but were no more frequent than in control brains (Fig. 5*B*). Thus, a lack of MKK7 does not impair the regulation of apoptosis in the developing brain.

We next investigated whether loss of MKK7 caused any alterations to neuronal differentiation. Cortical neurons can be identified by immunostaining with antibodies recognizing neuronal markers such as Brn2, Satb2, Ctip2, Foxp2, and Tbr2 (Bulfone et al., 1999; McEvilly et al., 2002; Ferland et al., 2003; Arlotta et al., 2005; Britanova et al., 2005). We detected expression of all of these markers in *Mkk7*$^{flox/flox}$*Nestin-Cre* cortex (Fig. 5*C*,*D*), indicating that cortical neurons differentiate normally without MKK7. Next, because it was reported that the major JNK substrate c-Jun is involved in the specification of GABAergic/glutamatergic neurons in the spinal cord of *Xenopus tropicalis* (Marek et al., 2010), we performed an *in situ* hybridization analysis of *Mkk7*$^{flox/flox}$ *Nestin-Cre* spinal cord using probes for *gad1* and *vglut2*, which are expressed in GABAergic or glutamatergic neurons, respectively. However, no significant alterations to expression levels of *gad1* or *vglut2* were detected between control and *Mkk7*$^{flox/flox}$ *Nestin-Cre* mice (data not shown). These data show that, as was true for cortical neurons, the differentiation of GABAergic and glutamatergic neurons is not affected by MKK7 deletion.

Delayed neuronal radial migration

Previous reports showed that overexpression of dominant-negative JNK or MKK4 disruption can delay neuronal radial migration in the cerebral cortex (Kawauchi et al., 2003; Wang et al., 2007). To determine whether MKK7 also affects this process, we performed a timed pregnancy study of BrdU incorporation in the developing cerebral cortex. Embryos were labeled *in utero* with BrdU at E15.5 and brain sections prepared at E18.5 were immunostained with anti-BrdU antibody. We found that, in *Mkk7*$^{flox/flox}$ *Nestin-Cre* brain, BrdU-positive cells were dispersed throughout the ventricular zone (VZ), intermediate zone, and cortical plate, with a small proportion of BrdU-positive cells located in Bin1. In control brain, a significantly larger proportion of BrdU-positive cells was located in Bin1 (Fig. 6*A*,*B*). Thus, like MKK4, MKK7 influences the radial migration of neurons in the cortex.

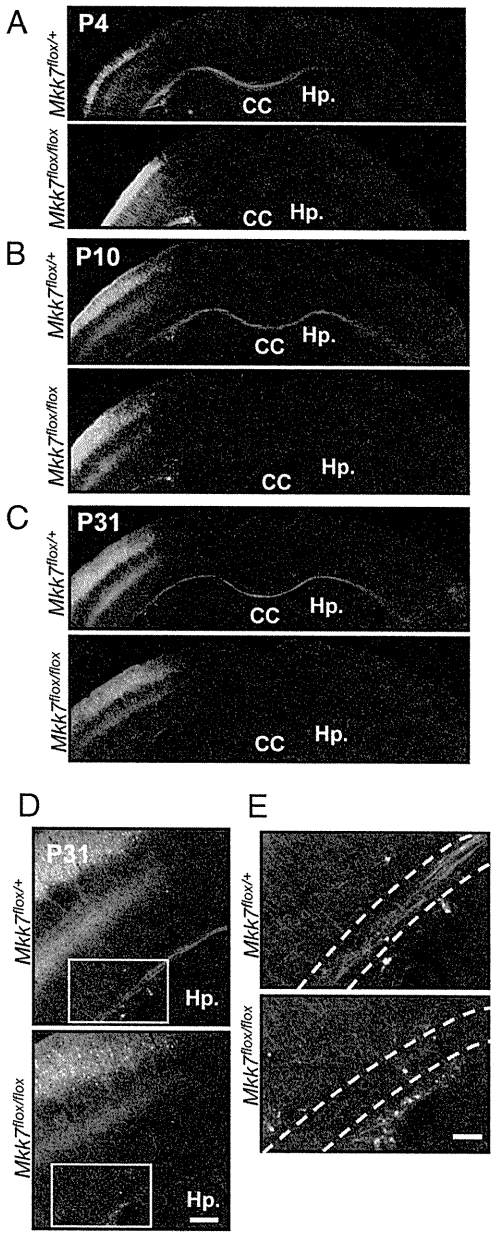

Figure 7. Deletion of *mkk7* in layer 2/3 neurons prevents axon elongation *in vivo*. ***A–C***, Layer-specific MKK7 deletion. pCAG-NLS-Cre and pCAG-floxed-polyA-EGFP were introduced by *in utero* electroporation into the VZ of control *Mkk7*$^{flox/+}$ and *Mkk7*$^{flox/flox}$ embryos at E15.5. Brains were fixed on the indicated postnatal days and coronal sections of the cortex were immunostained with anti-GFP antibody. Hp., Hippocampus. Scale bar, 1 mm. ***D***, Higher-magnification view of axons in the cortices of the *Mkk7*$^{flox/+}$ and *Mkk7*$^{flox/flox}$ mice in ***C***. Scale bar, 200 μm. ***E***, Higher-magnification view of the inset boxes in ***D***, focusing on the white matter (broken lines). Scale bar, 100 μm.

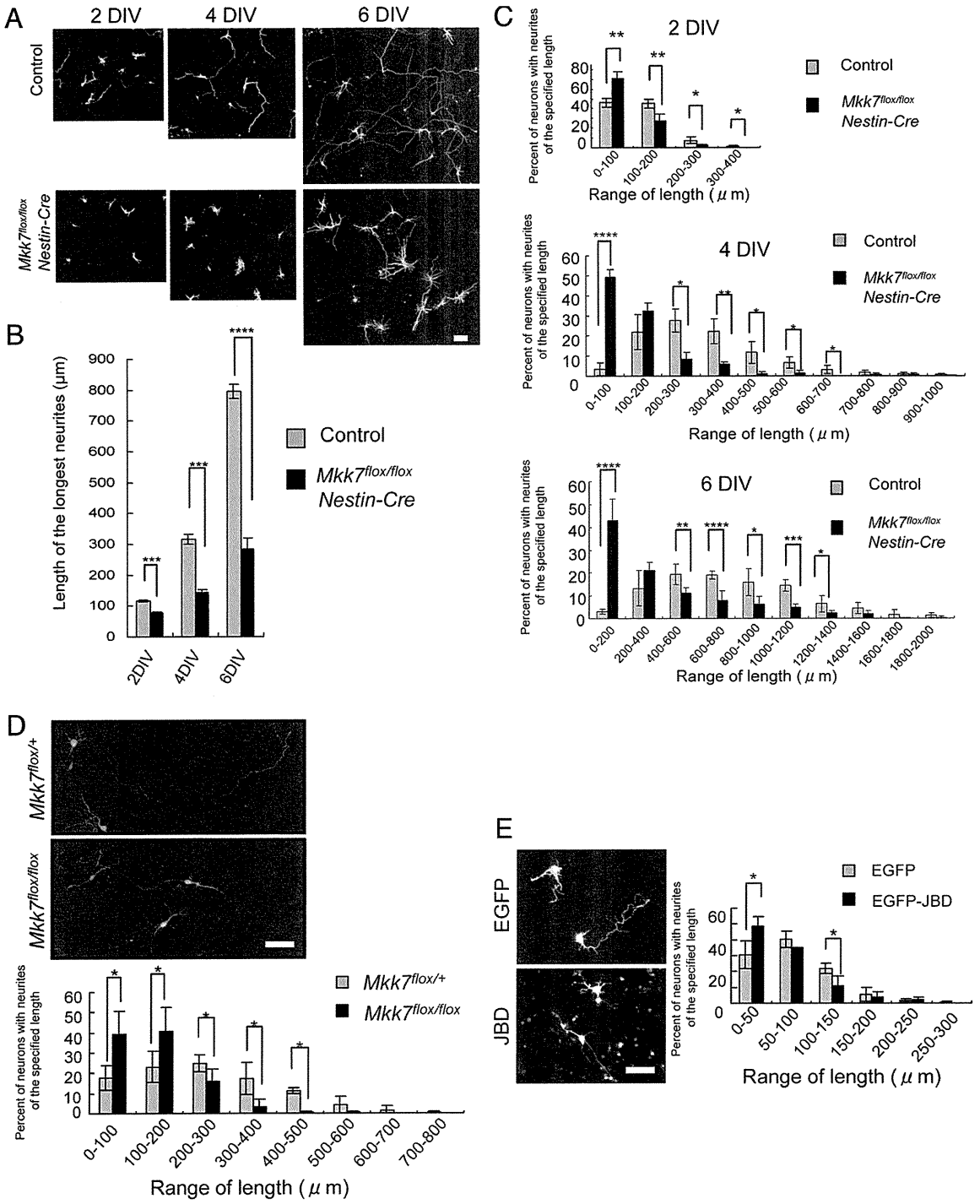

Figure 8. Deletion of *mkk7* in layer 2/3 neurons reduces neurite length *in vitro*. ***A–C***, Reduced axon elongation. The VZ of control ($n = 6$) and *Mkk7*$^{flox/flox}$ *Nestin-Cre* ($n = 3$) embryos at E15.5 was electroporated with pCAG-EGFP. Brains were dissected at E16.5 and primary neuron cultures were established. ***A***, After 2, 4, or 6 DIV, neurons were fixed and stained with anti-GFP antibody (upper panels; scale bar, 100 μm). ***B***, The lengths of the longest neurites of individual neurons in the cultures in ***A*** were measured at 2, 4, and 6 DIV (>100 neurons examined in each 2 DIV and 4 DIV culture, and >40 neurons in each 6 DIV culture). The results are plotted as a histogram and are the mean ± SE for each time point (*Mkk7*$^{flox/flox}$ *Nestin-Cre*, $n = 3$; control, $n = 6$). ***C***, The distribution of the longest neurite lengths was plotted for each set of cultures in ***A***. Results are the mean ± SD (*Mkk7*$^{flox/flox}$ *Nestin-Cre*, $n = 3$; control, $n = 6$). ***D***, Cell-autonomous defect. The VZ of control and *Mkk7*$^{flox/flox}$ embryos at E15.5 was electroporated with pCAG-NLS-Cre plus pCAG-floxed-polyA-EGFP, and primary neuron cultures were established at E16.5. After 4 DIV, neurons were fixed and stained with anti-GFP-antibody (upper; scale bar, 50 μm). The lengths of the longest neurites of individual neurons were measured, and the distribution of these lengths was plotted (lower). Results are the mean ± SD ($n = 3$). ***E***, Effect of JNK inhibition. The VZ of WT embryos at E15.5 was electroporated with pCAG-EGFP or pCAG-EGFP-JBD, and primary neuron cultures were established at E16.5. After 2 DIV, neurons were fixed and stained (left; scale bar, 50 μm). The distribution of neurite lengths was analyzed as for ***E*** (right). Results are the mean ± SD ($n = 3$). For ***A–D***, $^{*}p < 0.05$, $^{***}p < 0.001$, $^{****}p < 0.0001$.

MKK7 deletion in layer 2/3 neurons results in the disappearance of contralateral projecting axons *in vivo*

Our immunostaining experiments indicated that axon tracts were abnormal in the absence of MKK7. However, axon elongation is regulated not only by the neuron itself but also by environmental factors such as nerve growth factors. To determine whether the axon defect, we observed was due to the effects of MKK7 deletion on neuronal axon elongation or on environmental factors, we generated mice in which MKK7 disruption was induced specifically in layer 2/3 neurons. We used *in utero* elec-

troporation to introduce pCAG-NLS-Cre and its reporter plasmid pCAG-floxed-polyA-EGFP into the VZ of control and *Mkk7*$^{flox/flox}$ embryos at E15.5. We then killed the pups at P4, P10, or P31 and examined them for GFP fluorescence (representing successful Cre recombination). GFP-positive neurons were detected in layer 2/3 neurons in both *Mkk7*$^{flox/+}$ and *Mkk7*$^{flox/flox}$ brains through all postnatal stages examined. However, unlike controls, GFP-positive neurons in *Mkk7*$^{flox/flox}$ brain were not able to elongate axons to reach the contralateral cortex by P4 (Fig. 7*A*), nor was contralateral elongation detected at P10 or P31 in the mutant brains (Fig. 7*B*,*C*). Interestingly, when we investigated the morphology of these faulty axons in detail at P31, we found that both control and *Mkk7*$^{flox/flox}$ layer 2/3 neurons were able to elongate axons radially in the cerebral cortex such that their branches projected to layer 5 (Fig. 7*D*). However, in the mutant brain, axons running tangentially in the white matter had disappeared (Fig. 7*E*). When we attempted to determine whether the disappearance of these contralaterally projecting axons was due to a failure in axon guidance, we found no evidence of an axon guidance defect (data not shown). These results show *in vivo* that MKK7 regulates axon elongation in a cell-autonomous manner, and that MKK7 is required for the contralateral projection of axons of layer 2/3 neurons in the white matter.

We also examined axon elongation of layer 2/3 neurons *in vitro*. We introduced GFP into control and *Mkk7*$^{flox/flox}$ *Nestin-Cre* brains by *in utero* electroporation at E15.5 and prepared cultures of dissociated neurons at E16.5. We then measured the lengths of the longest neurites appearing in the cultures and found that there were more neurons with shorter neurites in *Mkk7*$^{flox/flox}$ *Nestin-Cre* cultures after 2, 4, or 6 d *in vitro* culture (DIV) compared with control cultures (Fig. 8*A–C*). To determine whether this defect in axon growth was induced a cell-autonomous manner, we disrupted MKK7 in *Mkk7*$^{flox/flox}$ layer 2/3 neurons using *in utero* electroporation of NLS-Cre and floxed-polyA-EGFP, and cultured control and mutant GFP-positive neurons for 4 d. Upon measurement of the longest neurites appearing in these cultures, we found that there were more neurons with shorter neurites in *Mkk7*$^{flox/flox}$ cultures at 4 DIV compared with *Mkk7*$^{flox/+}$ cultures (Fig. 8*D*). These results confirm *in vitro* that MKK7 regulates axon elongation in a cell-autonomous manner.

To determine whether our observations were due to effects on JNK signaling, we investigated whether inhibition of JNK caused the same neuronal phenotype as MKK7 disruption. WT layer 2/3 neurons were prepared after *in utero* electroporation of a plasmid expressing the JNK binding domain of JIP1 (JBD), which acts as a JNK inhibitory peptide (Westerlund et al., 2011). We found that, like MKK7 deletion, JNK inhibition resulted in more neurons with shorter axons (Fig. 8*E*). These results support our hypothesis that MKK7's effects on axon elongation are likely due to MKK7's regulation of its downstream target JNK.

Reduced phosphorylation of cytoskeletal components

We next determined whether the loss of MKK7 in neurons altered the phosphorylation of JNK substrates. Because phosphorylation of c-Jun was reduced in *Mkk7*$^{flox/flox}$ *Nestin-Cre* neurons (Fig. 9*A*), we performed rescue experiments in which plasmids expressing MKK7, MKK4, MKK7-JNK fusion protein (constitutively active JNK), or c-Jun were coelectroporated along with NLS-Cre and floxed-polyA-mCherry or -GFP into the VZ of E15.5 control and mutant embryos. Coelectroporation of MKK7 (Fig. 9*B*) and constitutively active JNK (Fig. 9*D*) allowed mutant neurons to recover their ability to contralaterally elongate axons, but the same was not true for coelectroporation of either MKK4 (Fig. 9*C*) or c-Jun (Fig. 9*E*). These data

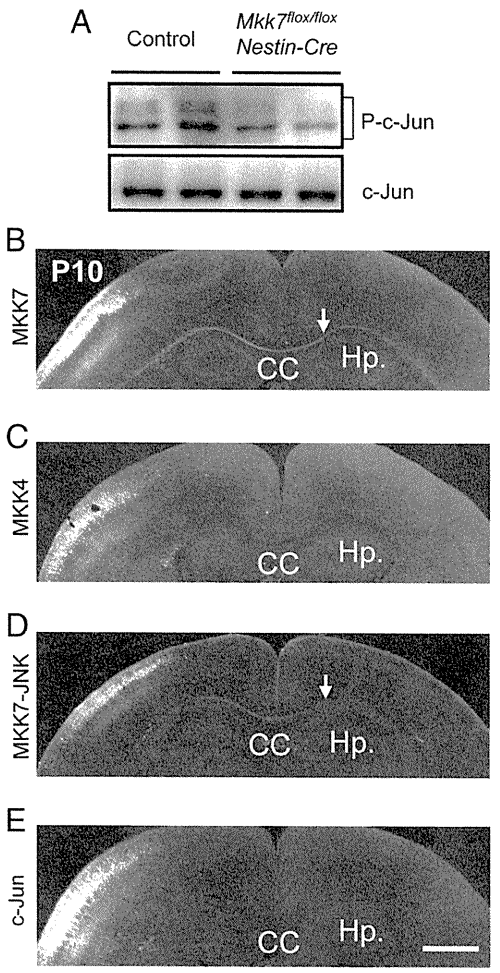

Figure 9. Contralateral axon projection is rescued by electroporation of MKK7 and active-JNK but not by MKK4 or c-Jun. ***A***, Decreased c-Jun phosphorylation. Brain extracts prepared from control and *Mkk7*$^{flox/flox}$ *Nestin-Cre* embryos at E18.5 were immunoblotted to detect total c-Jun and phospho-c-Jun. ***B–E***, Reversal of effects of MKK7 disruption. pCAG-NLS-Cre and pCAG-floxed-polyA-mCherry or -GFP were coelectroporated along with MKK7 (0.25 mg/ml) (***B***), MKK4 (0.25 mg/ml) (***C***), MKK7-JNK (0.05 mg/ml) (***D***), or c-Jun (1.0 mg/ml) (***E***) into the VZ of control and *Mkk7*$^{flox/flox}$ embryos at E15.5. Brains were fixed at P10 and coronal sections of cortices were immunostained with anti-RFP or GFP antibody. Arrows indicate axons rescued by coelectroporation. Hp, Hippocampus. Scale bar, 1 mm.

suggest that MKK7 regulates axon elongation through JNK, but that this signaling pathway does not involve transcription mediated by c-Jun.

In *Mkk4*$^{flox/flox}$ *Nestin-Cre* mice, the phosphorylation of certain neurofilament and MAPs is reportedly altered (Wang et al., 2007). Neurofilament heavy chain (NF-H) is a neuron-specific intermediate filament whose C-terminal tail is constitutively phosphorylated in axons by several proline-directed kinases, including JNK. When we investigated phosphorylation levels of NF-H in *Mkk7*$^{flox/flox}$ *Nestin-Cre* brain, we found that NF-H phosphorylation was reduced (Fig. 10*A*). The axon elongation and radial migration required for normal brain development also rely on MAP-dependent regulation of microtubule dynamics, and MAP activity is controlled by phosphorylation mediated by a number of protein kinases, including JNK. When we tested whether MAP phosphorylation was altered in *Mkk7*$^{flox/flox}$ *Nestin-Cre* brain, we found that phosphorylation levels of MAP1B were reduced (Fig. 10*B*). In addition, the phosphorylation of doublecortin (DCX) was suppressed by loss of MKK7 (Fig. 10*C*), an alteration that does not occur after disruption of MKK4 (Wang et al., 2007). These data show that, within the developing brain, MKK7 regulates the phosphoryla-

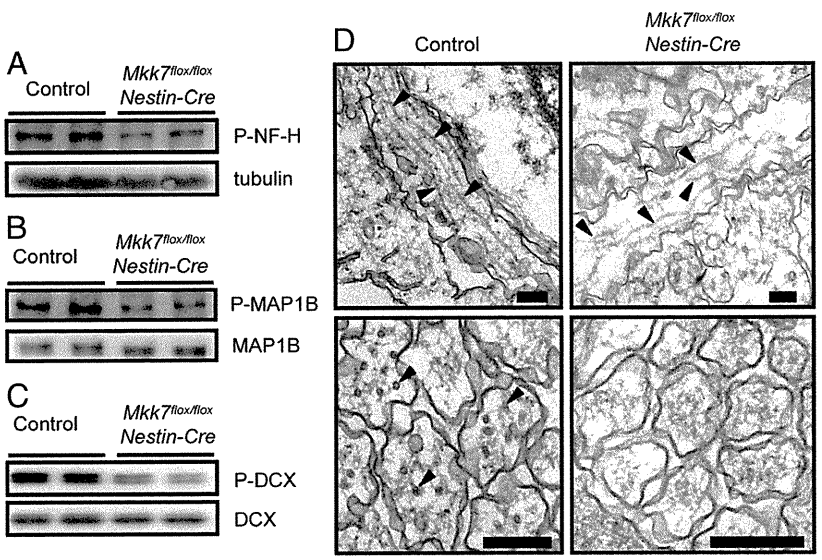

Figure 10. MKK7 regulates MAP phosphorylation. ***A–C***, Brain extracts from control and *Mkk7*$^{flox/flox}$ *Nestin-Cre* embryos at E18.5 were immunoblotted to detect phospho-NF-H and tubulin (loading control) (***A***); phospho-MAP1B and total MAP1B (***B***); and phospho-DCX and total DCX (***C***). ***D***, Defective microtubule structures in axons of *Mkk7*$^{flox/flox}$ *Nestin-Cre* brain. Electron micrographs of horizontal sections (upper) and cross-sections (lower) of axons in control and *Mkk7*$^{flox/flox}$*Nestin-Cre* brains are shown. Black arrowheads, Microtubules. Scale bars, 200 nm.

tion of not only NF-H and MAP1B, which are also regulated by MKK4, but also DCX.

We next examined whether microtubule stabilization could ameliorate the axonal defects caused by MKK7 disruption. Cultures of *Mkk7*$^{flox/flox}$ *Nestin-Cre* primary neurons were treated with Taxol, a drug that stabilizes microtubules and induces axon formation (Hirai et al., 2011). We found that Taxol treatment did indeed increase the lengths of axons in *Mkk7*$^{flox/flox}$ *Nestin-Cre* brain, but that these structures were still shorter than axons in Taxol-treated control cultures (data not shown). Finally, we examined microtubule structures in sections of axons directly by electron microscopy and found that *Mkk7*$^{flox/flox}$ *Nestin-Cre* brain contained axons with fewer and shorter microtubules than control brain (Fig. 10*D*). Thus, the regulatory effects of MKK7 on molecules critical for microtubule structures involve more than mere microtubule stabilization and do not overlap the effects of MKK4.

Discussion

Role of MKK7 in axon elongation

In this study, we investigated the physiological functions of MKK7 in the developing brain. Our most striking finding is that MKK7 regulates the elongation of axons by layer 2/3 neurons. *Mkk7*$^{flox/flox}$ *Nestin-Cre* brains displayed defective formation of axon tracts and decreased numbers of TAG-1-positive axons (Figs. 2, 4), a phenotype never observed in JNK-deficient mice. *Jnk1/2* double mutant mice die during early embryogenesis, precluding analysis of the developing brain. No brain defects have been reported for *Jnk2* and/or *Jnk3* knock-out mice (Hunot et al., 2004), and although *Jnk1*$^{-/-}$ mice display abnormalities of axon maintenance and radial migration, axon formation is normal in these mutants (Chang et al., 2003; Westerlund et al., 2011). These results indicate that there is redundancy among JNK1, 2, and 3 functions that obscures the effects of JNK signaling on axon elongation because all of these kinases are expressed in the brain. Our report on mice lacking the JNK activator MKK7 specifically in neural stem cells and postmitotic neurons is the first to demonstrate that JNK signaling regulates axon elongation *in vivo*.

By using *in utero* electroporation, we showed that MKK7 controls axon elongation in a cell-autonomous manner (Figs. 7, 8). Our work has also uncovered a very interesting phenotype affecting neuronal contralateral axon projection. It is well known that axons of layer 2/3 neurons run radially in the ipsilateral cortex to the white matter, and then run tangentially and project to the contralateral cortex. In the ipsilateral side, layer 2/3 axons normally extend branches projecting to layer 5 and form barrel nets, which are axonal trajectories made after the initial appearance of barrels (Sehara et al., 2010). In our study, layer 2/3 neurons lacking MKK7 did not extend axons running tangentially in the white matter or form contralateral projections, although the axons of these neurons did run radially in the ipsilateral cortex and formed branches and barrel nets (Fig. 7*D*,*E*). Our results suggest that axon elongation is regulated by different mechanisms in the cerebral cortex and in the white matter, and that MKK7 plays an important role only in the latter case.

Role of MKK7 in MAP regulation

Proper regulation of microtubule dynamics is critical for axon elongation and radial migration, and this control is mediated mainly by MAPs such as MAP1B and DCX that bind to microtubules and stabilize them. Double mutant mice such as the *Map1b/Tau* or *Dcx/doublecortin-like kinase* (*Dclk*) strains display axonal malformation during brain development (Takei et al., 2000; Koizumi et al., 2006). Importantly, the ability of MAPs to regulate microtubule dynamics depends on their phosphorylation by several protein kinases, including JNK (Kawauchi et al., 2003; Gdalyahu et al., 2004). Phosphorylation of a MAP protein induces its disassociation from microtubules, which causes the microtubules to enter a dynamic state. In our study, we found that the phosphorylation levels of both MAP1B and DCX were reduced (Fig. 10*B*,*C*), and that microtubule structures appeared abnormal in *Mkk7*$^{flox/flox}$ *Nestin-Cre* axons (Fig. 10*D*). Based on our results and the literature, we propose that MKK7-JNK signaling controls the phosphorylation of MAP1B and DCX that regulates microtubule dynamics, and that this phosphorylation may be one of several mechanisms promoting axon elongation.

Role of MKK7 in apoptosis

It has been previously reported that *Jnk1/Jnk2* double mutant mice are embryonic lethal at E11.5 due to severely dysregulated apoptosis in the brain (Kuan et al., 1999; Sabapathy et al., 1999). The results of these studies indicated that JNK regulates apoptosis positively in the forebrain and negatively in the hindbrain during early brain development. However, when we examined the regulation of apoptosis in our *Mkk7*$^{flox/flox}$ *Nestin-Cre* mice, we found no abnormalities (Fig. 5), in line with previous analyses of *Mkk4*$^{flox/flox}$ *Nestin-Cre* mice (Wang et al., 2007). One explanation for this discrepancy is that JNK signaling may regulate apoptosis during early brain development but is not involved in such apoptosis at later stages. Another possibility is that, because MKK4 remains intact in *MKK7*$^{flox/flox}$ *Nestin-Cre* brain, weak JNK

activation could have occurred that was sufficient for normal regulation of apoptosis in the developing brain. We are currently generating double conditional knock-out *Mkk7*$^{flox/flox}$/*Mkk4*$^{flox/flox}$ *Nestin-Cre* mice to resolve this issue.

Role of MKK7 in neuronal differentiation

When we investigated whether MKK7 was involved in neuronal differentiation, all markers examined were expressed with essentially normal distributions (Fig. 5). These results indicate that neuronal differentiation is not affected by MKK7 disruption in the cortex. We also determined whether MKK7 was involved in regulating the activity of c-Jun needed for neurotransmitter specification in the dorsal spinal cord. A recent study of *Xenopus tropicalis* demonstrated that c-Jun regulates neurotransmitter specification through transcriptional regulation of Tlx3 in the dorsal spinal cord of this animal (Marek et al., 2010). This group showed that c-Jun activation induces the formation of GABAergic neurons and suppresses glutamatergic differentiation. Because c-Jun is a major substrate of JNK, we hypothesized that we might see a reduction of GABAergic neurons and an increase in glutamatergic neurons in the spinal cords of *Mkk7*$^{flox/flox}$ *Nestin-Cre* mice due to suppression of c-Jun activity caused by the lack of MKK7. However, our *in situ* hybridization analysis of *gad1* and *vglut2* expression showed no alterations in the dorsal spinal cords of *Mkk7*$^{flox/flox}$ *Nestin-Cre* mice (data not shown). Thus, neurotransmitter specification is not influenced by MKK7 deletion. It remains possible that low levels of c-Jun phosphorylation still occurred in *Mkk7*$^{flox/flox}$ *Nestin-Cre* mice that were sufficient for normal neurotransmitter specification. Alternatively, GABAergic/glutamatergic differentiation may be regulated by different mechanisms in *Xenopus tropicalis* and *Mus musculus*.

Ultrastructural alterations in *Mkk7*$^{flox/flox}$ *Nestin-Cre* mice

Electron microscopy revealed abnormal accumulations of intermediate filaments in the axons of *Mkk7*$^{flox/flox}$ *Nestin-Cre* brain (Fig. 3*A*), as well as reduced phosphorylation of NF-H (Fig. 10*A*). NF-H is a neuron-specific intermediate filament, and it has been reported that the C-terminal tail of NF-H regulates interactions among NFs and influences their axonal transport (Sasaki et al., 2009; Lee et al., 2011). It is therefore possible that JNK-mediated phosphorylation of NF-H is required for normal NF-H distribution, and that failure of this regulation due to loss of MKK7 induces the accumulation of filamentous structures within axons. Our electron microscopy analyses also showed that *Mkk7*$^{flox/flox}$ *Nestin-Cre* brain contained numerous autophagic vacuoles (Fig. 3*B*). Although it is possible that autophagy is a secondary effect induced by the abnormal accumulation of intermediate filaments in our mutants, it has been reported that JNK signaling is directly involved in the formation of autophagic vacuoles and autophagic cell death (Byun et al., 2009; Shimizu et al., 2010; Kim et al., 2011; Xu et al., 2011). We are currently studying our *Mkk7*$^{flox/flox}$ *Nestin-Cre* mice to determine whether MKK7-JNK signaling acts to suppress autophagy in the developing brain.

Comparison of MKK4 and MKK7 in the developing brain

MKK7 and MKK4 are both JNK activators, and complete activation of JNK requires the activities of both of these kinases (Kishimoto et al., 2003). In our *Mkk7*$^{flox/flox}$ *Nestin-Cre* mice, phosphorylated JNK was markedly reduced despite an upregulation of MKK4 (Fig. 1*E*). This result is consistent with that of Wang and colleagues, who showed that MKK4 deletion decreases JNK activation to 1/5 of control values (Wang et al., 2007). Together, these findings suggest that both MKK7 and MKK4 are required for optimal JNK activation in the developing brain. Furthermore, this optimal JNK activation is essential for normal neuronal radial migration in the cortex, since both *Mkk7*$^{flox/flox}$ *Nestin-Cre* mice (Fig. 6) and *Mkk4*$^{flox/flox}$ *Nestin-Cre* mice (Wang et al., 2007) show defects in this process. However, other phenotypes do not overlap between *MKK7*$^{flox/flox}$ *Nestin-Cre* and *Mkk4*$^{flox/flox}$ *Nestin-Cre* mice. *Mkk7*$^{flox/flox}$ *Nestin-Cre* mice die at birth (Table 1, Fig. 1*F*), whereas *Mkk4*$^{flox/flox}$ *Nestin-Cre* mice survive until age 3 weeks. *Mkk7*$^{flox/flox}$ *Nestin-Cre* mice (E18.5) display enlarged brain ventricles, diminished striatum, decreased forebrain axon tracts, and reduced corticofugal axons (Figs. 2, 4), but none of these defects has been observed (or at least has not been reported) for *Mkk4*$^{flox/flox}$ *Nestin-Cre* mice. Thus, MKK7 has unique functions in the developing brain that differ from those of MKK4.

Differences between MKK7 and MKK4 functions also appear at the molecular level. In *Mkk4*$^{flox/flox}$ *Nestin-Cre* brain, phosphorylation levels of MAP1B are reduced, but DCX phosphorylation is not altered (Wang et al., 2007). In contrast, we found that the phosphorylation levels of both MAP1B and DCX were reduced in *Mkk7*$^{flox/flox}$ *Nestin-Cre* brain (Fig. 10*B*,*C*), suggesting a difference in substrates affected by MKK7-JNK versus MKK4-JNK signaling. In line with this hypothesis, the scaffold protein JIP1 binds to JNK, MKK7, and DCX but not to MKK4 (Whitmarsh et al., 1998; Wang et al., 2007). We therefore propose that differences in scaffold proteins and/or substrates involved in MKK7-JNK versus MKK4-JNK signaling pathways could cause the phenotypic divergence observed between *Mkk7*$^{flox/flox}$ *Nestin-Cre* and *Mkk4*$^{flox/flox}$ *Nestin-Cre* mice.

In conclusion, our results reveal an important and unique role for MKK7 during axon elongation in the developing brain, and reinforce the complex nature of JNK signaling and regulation *in vivo*.

References

Arlotta P, Molyneaux BJ, Chen J, Inoue J, Kominami R, Macklis JD (2005) Neuronal subtype-specific genes that control corticospinal motor neuron development in vivo. Neuron 45:207–221.

Asaoka Y, Nishina H (2010) Diverse physiological functions of MKK4 and MKK7 during early embryogenesis. J Biochem 148:393–401.

Björkblom B, Ostman N, Hongisto V, Komarovski V, Filén JJ, Nyman TA, Kallunki T, Courtney MJ, Coffey ET (2005) Constitutively active cytoplasmic c-Jun N-terminal kinase 1 is a dominant regulator of dendritic architecture: role of microtubule-associated protein 2 as an effector. J Neurosci 25:6350–6361.

Britanova O, Akopov S, Lukyanov S, Gruss P, Tarabykin V (2005) Novel transcription factor Satb2 interacts with matrix attachment region DNA elements in a tissue-specific manner and demonstrates cell-type-dependent expression in the developing mouse CNS. Eur J Neurosci 21:658–668.

Bulfone A, Martinez S, Marigo V, Campanella M, Basile A, Quaderi N, Gattuso C, Rubenstein JL, Ballabio A (1999) Expression pattern of the Tbr2 (Eomesodermin) gene during mouse and chick brain development. Mech Dev 84:133–138.

Byun JY, Yoon CH, An S, Park IC, Kang CM, Kim MJ, Lee SJ (2009) The Rac1/MKK7/JNK pathway signals upregulation of Atg5 and subsequent autophagic cell death in response to oncogenic Ras. Carcinogenesis 30:1880–1888.

Chang L, Karin M (2001) Mammalian MAP kinase signalling cascades. Nature 410:37–40.

Chang L, Jones Y, Ellisman MH, Goldstein LSB, Karin M (2003) JNK1 is required for maintenance of neuronal microtubules and controls phosphorylation of microtubule-associated proteins. Dev Cell 4:521–533.

Davis RJ (2000) Signal transduction by the JNK group of MAP kinases. Cell 103:239–252.

Denaxa M, Chan CH, Schachner M, Parnavelas JG, Karagogeos D (2001) The adhesion molecule TAG-1 mediates the migration of cortical interneurons from the ganglionic eminence along the corticofugal fiber system. Development 128:4635–4644.

Enslen H, Raingeaud J, Davis RJ (1998) Selective activation of p38 mitogen-activated protein (MAP) kinase isoforms by the MAP kinase kinases MKK3 and MKK6. J Biol Chem 273:1741–1748.

Ferland RJ, Cherry TJ, Preware PO, Morrisey EE, Walsh CA (2003) Characterization of Foxp2 and Foxp1 mRNA and protein in the developing and mature brain. J Comp Neurol 460:266–279.

Gdalyahu A, Ghosh I, Levy T, Sapir T, Sapoznik S, Fishler Y, Azoulai D, Reiner O (2004) DCX, a new mediator of the JNK pathway. EMBO J 23:823–832.

Hibi M, Lin A, Smeal T, Minden A, Karin M (1993) Identification of an oncoprotein- and UV-responsive protein kinase that binds and potentiates the c-Jun activation domain. Genes Dev 7:2135–2148.

Hirai S, Banba Y, Satake T, Ohno S (2011) Axon formation in neocortical neurons depends on stage-specific regulation of microtubule stability by the dual leucine zipper kinase-c-Jun N-terminal kinase pathway. J Neurosci 31:6468–6480.

Hunot S, Vila M, Teismann P, Davis RJ, Hirsch EC, Przedborski S, Rakic P, Flavell RA (2004) JNK-mediated induction of cyclooxygenase 2 is required for neurodegeneration in a mouse model of Parkinson's disease. Proc Natl Acad Sci U S A 101:665–670.

Imai F, Hirai S, Akimoto K, Koyama H, Miyata T, Ogawa M, Noguchi S, Sasaoka T, Noda T, Ohno S (2006) Inactivation of aPKClambda results in the loss of adherens junctions in neuroepithelial cells without affecting neurogenesis in mouse neocortex. Development 133:1735–1744.

Ito M, Yoshioka K, Akechi M, Yamashita S, Takamatsu N, Sugiyama K, Hibi M, Nakabeppu Y, Shiba T, Yamamoto KI (1999) JSAP1, a novel jun N-terminal protein kinase (JNK)-binding protein that functions as a scaffold factor in the JNK signaling pathway. Mol Cell Biol 19:7539–7548.

Kawasaki H, Mizuseki K, Nishikawa S, Kaneko S, Kuwana Y, Nakanishi S, Nishikawa SI, Sasai Y (2000) Induction of midbrain dopaminergic neurons from ES cells by stromal cell-derived inducing activity. Neuron 28:31–40.

Kawauchi T, Chihama K, Nabeshima Y, Hoshino M (2003) The in vivo roles of STEF/Tiam1, Rac1 and JNK in cortical neuronal migration. EMBO J 22:4190–4201.

Kim MJ, Woo SJ, Yoon CH, Lee JS, An S, Choi YH, Hwang SG, Yoon G, Lee SJ (2011) Involvement of autophagy in oncogenic K-Ras-induced malignant cell transformation. J Biol Chem 286:12924–12932.

Kishimoto H, Nakagawa K, Watanabe T, Kitagawa D, Momose H, Seo J, Nishitai G, Shimizu N, Ohata S, Tanemura S, Asaka S, Goto T, Fukushi H, Yoshida H, Suzuki A, Sasaki T, Wada T, Penninger JM, Nishina H, Katada T (2003) Different properties of SEK1 and MKK7 in dual phosphorylation of stress-induced activated protein kinase SAPK/JNK in embryonic stem cells. J Biol Chem 278:16595–16601.

Koizumi H, Tanaka T, Gleeson JG (2006) Doublecortin-like kinase functions with doublecortin to mediate fiber tract decussation and neuronal migration. Neuron 49:55–66.

Kuan CY, Yang DD, Samanta Roy DR, Davis RJ, Rakic P, Flavell RA (1999) The Jnk1 and Jnk2 protein kinases are required for regional specific apoptosis during early brain development. Neuron 22:667–676.

Lee S, Sunil N, Shea TB (2011) C-terminal neurofilament phosphorylation fosters neurofilament-neurofilament associations that compete with axonal transport. Cytoskeleton (Hoboken) 68:8–17.

Marek KW, Kurtz LM, Spitzer NC (2010) cJun integrates calcium activity and tlx3 expression to regulate neurotransmitter specification. Nat Neurosci 13:944–950.

McEvilly RJ, de Diaz MO, Schonemann MD, Hooshmand F, Rosenfeld MG (2002) Transcriptional regulation of cortical neuron migration by POU domain factors. Science 295:1528–1532.

Nakagawa K, Sugahara M, Yamasaki T, Kajiho H, Takahashi S, Hirayama J, Minami Y, Ohta Y, Watanabe T, Hata Y, Katada T, Nishina H (2010) Filamin associates with stress signalling kinases MKK7 and MKK4 and regulates JNK activation. Biochem J 427:237–245.

Okada S, Nakamura M, Katoh H, Miyao T, Shimazaki T, Ishii K, Yamane J, Yoshimura A, Iwamoto Y, Toyama Y, Okano H (2006) Conditional ablation of Stat3 or Socs3 discloses a dual role for reactive astrocytes after spinal cord injury. Nat Med 12:829–834.

Sabapathy K, Jochum W, Hochedlinger K, Chang L, Karin M, Wagner EF (1999) Defective neural tube morphogenesis and altered apoptosis in the absence of both JNK1 and JNK2. Mech Dev 89:115–124.

Saito T (2006) In vivo electroporation in the embryonic mouse central nervous system. Nat Protoc 1:1552–1558.

Sasaki T, Ishiguro K, Hisanaga S (2009) Novel axonal distribution of neurofilament-H phosphorylated at the glycogen synthase kinase 3beta-phosphorylation site in its E-segment. J Neurosci Res 87:3088–3097.

Schramek D, Kotsinas A, Meixner A, Wada T, Elling U, Pospisilik JA, Neely GG, Zwick R-H, Sigl V, Forni G, Serrano M, Gorgoulis VG, Penninger JM (2011) The stress kinase MKK7 couples oncogenic stress to p53 stability and tumor suppression. Nat Genet 43:212–219.

Sehara K, Toda T, Iwai L, Wakimoto M, Tanno K, Matsubayashi Y, Kawasaki H (2010) Whisker-related axonal patterns and plasticity of layer 2/3 neurons in the mouse barrel cortex. J Neurosci 30:3082–3092.

Shimizu S, Konishi A, Nishida Y, Mizuta T, Nishina H, Yamamoto A, Tsujimoto Y (2010) Involvement of JNK in the regulation of autophagic cell death. Oncogene 29:2070–2082.

Tabata H, Nakajima K (2008) Labeling embryonic mouse central nervous system cells by in utero electroporation. Dev Growth Differ 50:507–511.

Takei Y, Teng J, Harada A, Hirokawa N (2000) Defects in axonal elongation and neuronal migration in mice with disrupted tau and map1b genes. J Cell Biol 150:989–1000.

Toda T, Hayakawa I, Matsubayashi Y, Tanaka K, Ikenaka K, Lu QR, Kawasaki H (2008) Termination of lesion-induced plasticity in the mouse barrel cortex in the absence of oligodendrocytes. Mol Cell Neurosci 39:40–49.

Ura S, Nishina H, Gotoh Y, Katada T (2007) Activation of the c-Jun N-terminal kinase pathway by MST1 is essential and sufficient for the induction of chromatin condensation during apoptosis. Mol Cell Biol 27:5514–5522.

Wada T, Nakagawa K, Watanabe T, Nishitai G, Seo J, Kishimoto H, Kitagawa D, Sasaki T, Penninger JM, Nishina H, Katada T (2001) Impaired synergistic activation of stress-activated protein kinase SAPK/JNK in mouse embryonic stem cells lacking SEK1/MKK4: different contribution of SEK2/MKK7 isoforms to the synergistic activation. J Biol Chem 276:30892–30897.

Wada T, Joza N, Cheng HY, Sasaki T, Kozieradzki I, Bachmaier K, Katada T, Schreiber M, Wagner EF, Nishina H, Penninger JM (2004) MKK7 couples stress signalling to G2/M cell-cycle progression and cellular senescence. Nat Cell Biol 6:215–226.

Wang X, Nadarajah B, Robinson AC, McColl BW, Jin JW, Dajas-Bailador F, Boot-Handford RP, Tournier C (2007) Targeted deletion of the mitogen-activated protein kinase kinase 4 gene in the nervous system causes severe brain developmental defects and premature death. Mol Cell Biol 27:7935–7946.

Westerlund N, Zdrojewska J, Padzik A, Komulainen E, Björkblom B, Rannikko E, Tararuk T, Garcia-Frigola C, Sandholm J, Nguyen L, Kallunki T, Courtney MJ, Coffey ET (2011) Phosphorylation of SCG10/stathmin-2 determines multipolar stage exit and neuronal migration rate. Nat Neurosci 14:305–313.

Whitmarsh AJ, Cavanagh J, Tournier C, Yasuda J, Davis RJ (1998) A mammalian scaffold complex that selectively mediates MAP kinase activation. Science 281:1671–1674.

Wolfer DP, Henehan-Beatty A, Stoeckli ET, Sonderegger P, Lipp HP (1994) Distribution of TAG-1/axonin-1 in fibre tracts and migratory streams of the developing mouse nervous system. J Comp Neurol 345:1–32.

Xu P, Das M, Reilly J, Davis RJ (2011) JNK regulates FoxO-dependent autophagy in neurons. Genes Dev 25:310–322.

Yasuda J, Whitmarsh AJ, Cavanagh J, Sharma M, Davis RJ (1999) The JIP group of mitogen-activated protein kinase scaffold proteins. Mol Cell Biol 19:7245–7254.

CLINICAL REPORT

AMERICAN JOURNAL OF medical genetics PART A

Axial Spondylometaphyseal Dysplasia: Additional Reports

Shigeru Suzuki,[1]* Ok-Hwa Kim,[2] Yoshio Makita,[3] Tetsuya Saito,[4] Gye-Yeon Lim,[5] Tae-Joon Cho,[6] Abdulrahman Al-Swaid,[7] Shatha Alrasheed,[7] Eiad Sadoon,[7] Osamu Miyazaki,[8] Sachiko Nishina,[9] Andrea Superti-Furga,[10] Sheila Unger,[11] Kenji Fujieda,[1] Shiro Ikegawa,[12] and Gen Nishimura[13]

[1]Department of Pediatrics, Asahikawa Medical University, Asahikawa, Japan

[2]Department of Radiology, Ajou University Hospital, Suwon, South Korea

[3]Education center, Asahikawa Medical University, Asahikawa, Japan

[4]Department of Ophthalmology, Hokkaido Medical Center for Child Health and Rehabilitation, Sapporo, Japan

[5]Department of Radiology, St. Mary's Hospital, The Catholic University, Seoul, South Korea

[6]Department of Orthopedic Surgery, Seoul National University Children's Hospital, Seoul, South Korea

[7]Department of Pediatrics, King Abdulaziz Medical City, Riyadh, Soudi Arabia

[8]Department of Radiology, National Center for Child Health and Development, Tokyo, Japan

[9]Department of Ophthalmology, National Center for Child Health and Development, Tokyo, Japan

[10]Department of Pediatrics, Centre Hospitalier Universitaire Vaudois, Lausanne, Switzerland

[11]Service of Medical Genetics, Centre Hospitalier Universitaire Vaudois, Lausanne, Switzerland

[12]Laboratory of Bone and Joint Diseases, Center for Genomic Medicine, RIKEN, Minato-ku, Tokyo, Japan

[13]Department of Pediatric Imaging, Tokyo Metropolitan Children's Medical Center, Tokyo, Japan

Received 31 March 2011; Accepted 8 June 2011

Axial spondylometaphyseal dysplasia (SMD) (OMIM 602271) is an uncommon skeletal dysplasia characterized by metaphyseal changes of truncal-juxtatruncal bones, including the proximal femora, and retinal abnormalities. The disorder has not attracted much attention since initially reported; however, it has been included in the nosology of genetic skeletal disorders [Warman et al. (2011); Am J Med Genet Part A 155A:943–968] in part because of a recent publication of two additional cases [Isidor et al. (2010); Am J Med Genet Part A 152A:1550–1554]. We report here on the clinical and radiological manifestations in seven affected individuals from five families (three sporadic cases and two familial cases). Based on our observations and Isidor's report, the clinical and radiological hallmarks of axial SMD can be defined: The main clinical findings are postnatal growth failure, rhizomelic short stature in early childhood evolving into short trunk in late childhood, and thoracic hypoplasia that may cause mild to moderate respiratory problems in the neonatal period and later susceptibility to airway infection. Impaired visual acuity comes to medical attention in early life and function rapidly deteriorates. Retinal changes are diagnosed as retinitis pigmentosa or pigmentary retinal degeneration on fundoscopic examination and cone-rod dystrophy on electroretinogram. The radiological hallmarks include short ribs with flared, cupped anterior ends, mild spondylar dysplasia, lacy iliac crests, and metaphyseal irregularities essentially confined to the proximal femora. Equally affected sibling pairs of opposite gender and parental consanguinity are strongly suggestive of autosomal recessive inheritance.

How to Cite this Article:
Suzuki S, Kim O-H, Makita Y, Saito T, Lim G-Y, Cho T-J, Al-Swaid A, Alrasheed S, Sadoon E, Miyazaki O, Nishina S, Superti-Furga A, Unger S, Fujieda K, Ikegawa S, Nishimura G. 2011. Axial spondylometaphyseal dysplasia: Additional reports.
Am J Med Genet Part A 9999:1–8.

Grant sponsor: Research on Child Health and Development; Grant sponsor: Ministry of Health, Labor and Welfare of Japan.
Shigeru Suzuki and Ok-Hwa Kim contributed equally to this work.
Kenji Fujieda deceased at March 19, 2010.
*Correspondence to:
Shigeru Suzuki, Department of Pediatrics, Asahikawa Medical University, 2-1-1-1 Midorigaoka Higashi, Asahikawa 078-8510, Japan.
E-mail: shige5p@asahikawa-med.ac.jp
Published online 00 Month 2011 in Wiley Online Library (wileyonlinelibrary.com).
DOI 10.1002/ajmg.a.34192

Key words: bone dysplasia; axial spondylometaphyseal dysplasia; retinitis pigmentosa

INTRODUCTION

The term spondylometaphyseal dysplasia (SMD) encompasses a heterogeneous group of disorders characterized by dysplastic changes in the metaphyses of tubular bones and metaphyseal equivalents of the spine and flat bones. Amongst the SMDs, the most common is SMD Kozlowski type (OMIM 184252), followed by SMD Sutcliffe (corner fracture) type (OMIM 184255), but there are also other rare types [Wirth, 2008]. Aside from SMD Kozlowski type, which is caused by heterozygous mutations in the transient receptor potential cation channel, subfamily V, member 4 gene (*TRPV4*) [Nishimura et al., 2010], the etiologies of the SMDs remain unknown. It is intriguing that certain types of SMDs present as a multi-system disorder, as exemplified by SMD with cone-rod dystrophy (OMIM 608940) [Sousa et al., 2008; Turell et al., 2010].

We previously reported on a new type of SMD, based on the clinical and radiologic observations in three children (a Japanese girl and two Korean siblings) [Ehara et al., 1997]. The disorder was termed "axial SMD", because the metaphyseal changes were confined to the truncal and juxtatruncal bones. The disorder was seen in association with ocular abnormalities, including retinitis pigmentosa (RP) and/or optic atrophy. Very recently, two additional cases have been reported confirming the axial SMD as a distinct entity [Isidor et al., 2010]. The Nosology Group of the International Skeletal Dysplasia Society included the disorder in "Nosology and classification of genetic skeletal disorders: 2010 version", and the group termed the entity SMD with retinal degeneration, axial type (OMIM 602271) [Warman et al., 2011]. With the addition of five newly identified cases (three sporadic patients and two siblings) and follow-up our previously reported sibling case, we are able to delineate the key clinical and radiographic features of this condition and hopefully facilitate the diagnosis of further individuals.

CLINICAL REPORTS

Patient 1

Patient 1 is a Japanese girl born to healthy, nonconsanguineous parents. Birth length was 47.6 cm (−1.0 SD). At birth, she had mild respiratory distress and a narrow thorax was noted. A tentative radiological diagnosis of Shwachman-Diamond syndrome was made. Ophthalmological screening at age 3 weeks disclosed RP (Fig. 1A), and no electrical activities were detectable by electroretinogram (ERG) at 4 months (Fig. 1B). Length at age 11 months was 64.3 cm (−3.4 SD).

Patient 2 and 3 (siblings)

Patients 2 and 3 have consanguineous parents (first cousins) of Saudi Arabian origin who also have four healthy children.

Patient 2, a girl, was born by vaginal delivery at 40 weeks' gestation after an unremarkable pregnancy. Apgar scores were 9 and 10 at 1 and 5 min, respectively. Birth length was 51 cm, and weight 3,440 g (both at 50th centile). At age 4 months, she was noted to have micromelic short stature (<3rd centile) with rhizomelic shortening of the upper limbs and a narrow thorax with Harrison's grooves. At age 4 $^{7/12}$ years, height was 93.5 cm (−4.0 SD), and weight was 13.1 kg (−3.0 SD). Ophthalmological examination at age 1 year showed early signs of RP. She underwent ERG examinations twice at age 3 and 4 years, which showed no response to light flash stimulation indicative of advanced retinal dysfunction, and visually evoked response study showed delayed P100. At last examination, she had low visual acuity and no night vision but she was able to walk independently. Her visual acuity has deteriorated faster than her brother's.

Patient 3, the older brother of Patient 2, was born by vaginal delivery at 40 weeks' gestation after an unremarkable pregnancy. Apgar scores were 9 at 1 and at 5 min. Birth weight was 3,480 g, length was 51 cm, and OFC was 35 cm (all at 50th centile). He sat at age 6 months and walked at 10 months. His development was unremarkable except for visual dysfunction. He was noted to have RP at age 9 months. Mild hyperopia and astigmatism were found bilaterally at age 3 years. He had ERG three times at age 2 $^{9/12}$ years, 6 years, and 7 years, all of which showed abnormal response to light flash stimulation. However, visually evoked response study was not significantly affected. At age 3 $^{7/12}$ years, he was referred for genetic consultation because of failure to thrive, short stature, small chest, and visual problems. He showed micromelic short stature (<3rd centile) with rhizomelic shortening of the upper limbs and a narrow thorax with Harrison grooves. At age 7 years, height was 106.5 cm (−5.5 SD), weight was 18.5 kg (−2.5 SD), and OFC was 52.6 cm (−2.5 SD).

At last review, he had low visual acuity and no night vision but he was able to walk independently and could read with difficulty during daytime.

Patient 4

Patient 4 is a Korean boy, who was the second child of nonconsanguineous, healthy parents. He came to medical attention at age 5 years because of short stature; 102.7 cm (−1.6 SD). He had mild bowlegs and pectus excavatum. At that time, inward gaze of the eyes and impaired visual acuity were also noted. At age 6 years, mild RP was diagnosed on fundoscopic examination. Then, visual acuity progressively worsened. At age 9 years, vision was severely impaired (V.d. = 0.06; V.s. = 0.125). On last examination, at 10 years of age, he had proportionate short stature with a height of 125.8 cm (−2.0 SD). In addition, modest narrow thorax, mild thoracic scoliosis, and rhizomelic shortening of the upper limbs were seen (Fig. 2A).

Patient 5

Patient 5 is a Japanese boy born to healthy, nonconsanguineous parents. He was delivered at 41 weeks' gestation. Birth length was 48.5 cm (−0.9 SD), weight was 3,052 g (−0.2 SD), and OFC was 34.0 cm (+0.1 SD). A narrow thorax was noted at birth. Apgar scores were 7 at 1 min and 5 at 5 min. He had moderate respiratory distress with laryngomalacia necessitating oxygen therapy in the neonatal period. The laryngomalacia improved gradually over the course of the first year. He was given a radiological diagnosis of

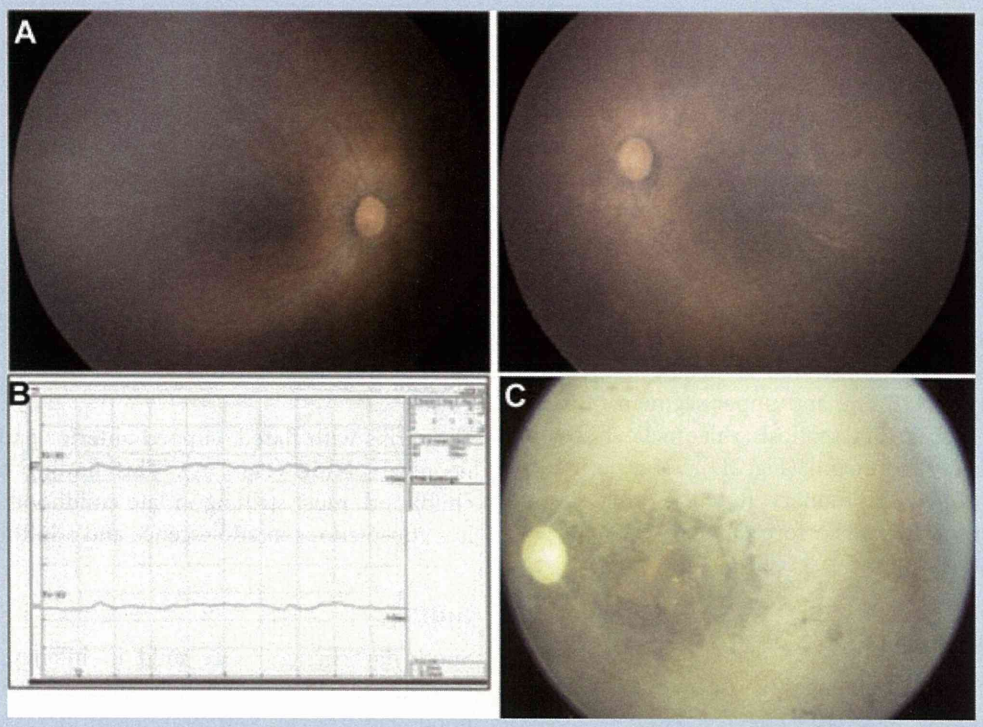

FIG. 1. Ophthalmological findings. A: in Patient 1, fundoscopy showed RP at age 2 months. B: in Patient 1, ERG did not trace electric activities at age 4 months. C: in Patient 5, fundoscopic findings were advanced RP with reduced retinal blood flow and optic nerve atrophy at age 12 years.

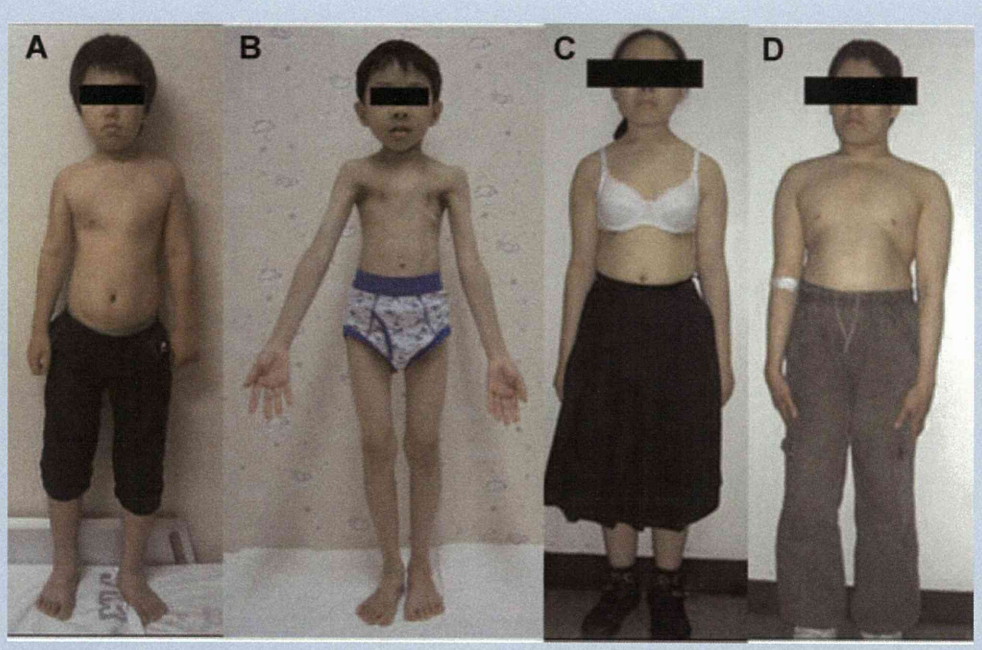

FIG. 2. Clinical photographs. A: Patient 4 at age 10 years. A mild narrow thorax and rhizomelic shortening of the upper limbs are noted. B: Patient 5 at age 12 years. Short trunk is striking with a mild narrow thorax. C: Patient 6 at age 15 years, (D) Patient 7 at age 23 years. Mild short trunk is evident, and the thorax is mildly narrow.

Jeune asphyxiating thoracic dysplasia in infancy. He had recurrent episodes of pneumonia until age 5 years. At age 6 years, severe short stature was recorded (−6.5 SD). Visual problems were suspected at an early age as he never showed any light response or the ability to track moving objects. Nystagmus was identified in early infancy. He was diagnosed as having macular RP at age 2 months. Visual evoked potential test showed no response. Severe hyperopia with disturbed visual acuity (V.d. = 0.01, V.s. = 0.01) was documented at age 5 years. Visual acuity gradually declined. He suffered from bilateral cataracts of the posterior subcapsular lense at 11 years. At age 12 years, fundoscopic findings showed advanced RP with reduced retinal blood flow and optic nerve atrophy (Fig. 1C). Clinical examination at that age demonstrated a height of 107.2 cm (−6.2 SD), arm span of 111.7 cm, and upper segment of 51 cm. He had a mild narrow thorax, mild scoliosis, rhizomelic shortening of the limbs, and markedly short trunk (Fig. 2D). Some permanent teeth had not yet erupted. Pulmonary function tests showed restrictive impairment with 38% forced vital capacity and 114.5% forced expiratory volume in 1 sec.

Patient 6 & 7 (siblings)

Patients 6 and 7 are Korean siblings, whose manifestations in childhood were previously reported [Ehara et al., 1997]. They were born to healthy, nonconsanguineous parents. Birth weight was normal. Short stature was noted in early childhood, as well as thoracic hypoplasia with susceptibility to airway infections. Height was 76 cm (−5.5 SD) at age 3 years in the younger sister, and 108 cm (−5.1 SD) at age 10 years in the older brother. The younger sister was diagnosed as having optic atrophy with nystagmus at age 3 years. Impaired visual acuity of the older brother came to attention at age 6 months, and he was diagnosed as having optic atrophy and retinal degeneration associated with nystagmus at age 8 years. At the most recent examination, the sister was 15 years, and the brother was 23 years old. Their heights were 131 cm (−5.1 SD) and 144 cm (−4.9 SD), respectively. They presented with a narrow thorax, short-trunk, and rhizomelic shortening of the upper limbs (Fig. 2C,D). They were functionally blind at that time.

RADIOLOGICAL FINDINGS

The radiographic findings in all patients were similar but with a variable degree of severity. The phenotype evolved with age.

Chest

Short ribs with flared, cupped anterior ends were evident in the neonatal period (Fig. 3A). This finding became prominent in childhood, most striking in late childhood (Fig. 3B–I), and then less conspicuous in adolescence and adulthood (Fig. 3J,K).

Spine

Spondylar changes were mild in infancy and early childhood (Fig. 4A–D). Platyspondyly became more apparent in late childhood (Fig. 4E–H). Vertebral height increased in adolescence and normalized in adulthood (Fig. 4I,J).

Pelvis

Lacy ilia were discernible in the neonatal period and became overt in childhood. Metaphyseal irregularities of the proximal femora became manifest in infancy and then progressed. Coxa vara devel-

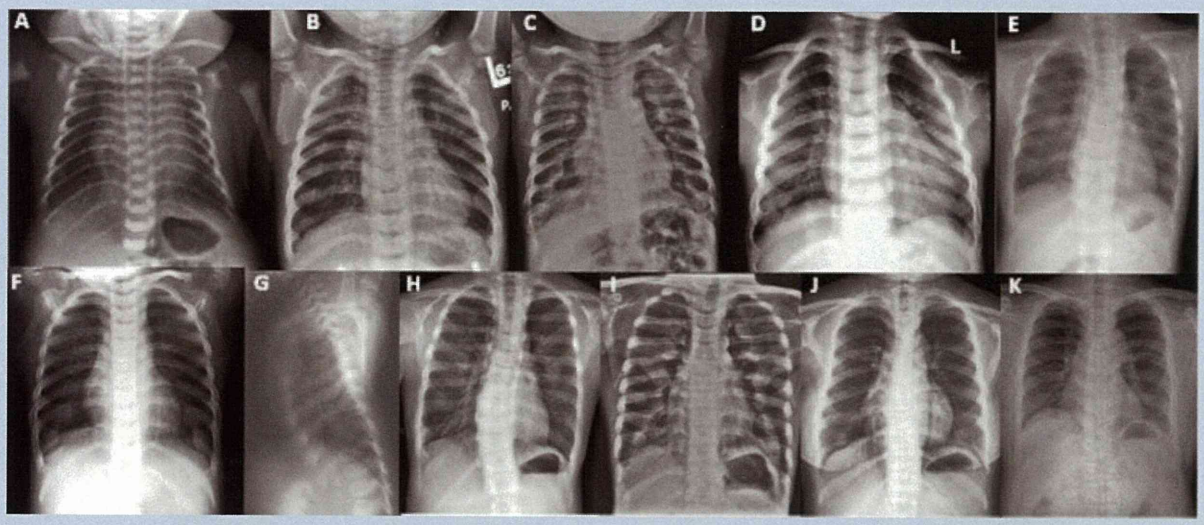

FIG. 3. Radiographs of the chest. A: Patient 1 at age 2 days, (B) Patient 2 at age $1^{4/12}$ years, (C) Patient 5 at age 2 years, (D) Patient 3 at age 4 years, (E) Patient 4 at age 5 years, (F) and (G) Patient 6 at age 8 years. Note a narrow thorax in (A), (C–E), and short ribs with cupped, flared anterior ends in all. Thoracic narrowing is modest in (B) and (F). Mild irregularities of the proximal humeral metaphyses are seen in (A,B) and (C). H: Patient 4 at age 10 years, (I) Patient 5 at age 12 years. Cupping and flaring of the anterior ends of the ribs are most conspicuous in late childhood. Thoracic narrowing is modest. J: Patient 6 at age 15 years, (K) Patient 7 at 23 age years. A narrow thorax is persistent, but cupping and flaring of the anterior ends of the ribs are less conspicuous than those at younger ages.

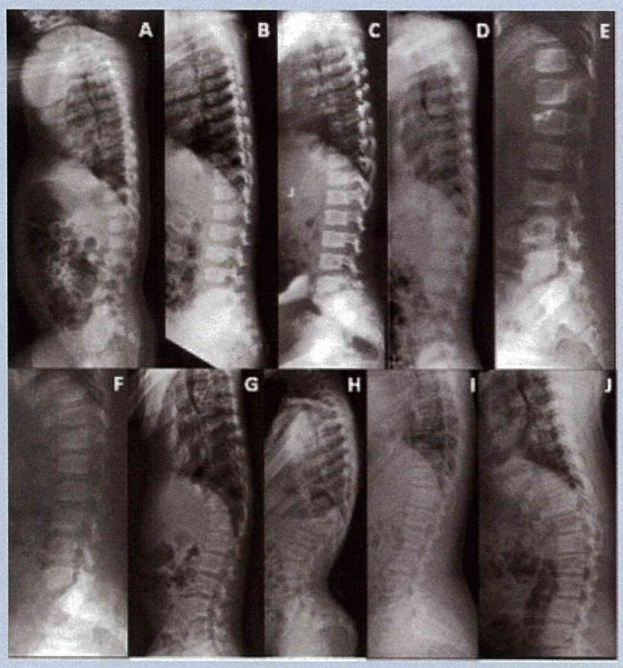

FIG. 4. Radiographs of spine. A: Patient 1 at age 6 months. The vertebral bodies are somewhat ovoid, but platyspondyly is not evident. B: Patient 2 at age 1 $^{4/12}$ years, (C) Patient 3 at age 4 years, (D) Patient 4 at age 5 years. Mild platyspondyly is evident. E: Patient 6 at 8 age years, (F) Patient 7 at age 10 years, (G) Patient 4 at age 10 years, (H) Patient 5 at age 12 years. Platyspondyly is most conspicuous in late childhood. I: Patient 6 at age 15 years, (J) Patient 7 at age 23 years. Platyspondyly is discernible but milder than that in childhood.

oped in late childhood (Fig. 5A–I). The iliac and metaphyseal changes diminished during adolescence, leaving only coxa vara (Fig. 5J,K).

Limbs

The proximal humeri showed mild metaphyseal irregularities (Fig. 3 A–C). Metaphyseal changes were absent or very mild in the knee (Fig. 6A–G).

Hands

Hands were unremarkable in all patients (data not shown).

DISCUSSION

Based on our experiences and the observations reported by Isidor et al. [2010], it is clear that axial SMD is a distinctive disease entity with recognizable clinical and radiographic features. "A new form of oculoskeletal syndrome" reported by Megarbane et al. [2004] may represent the same disorder. The clinical manifestations of the present and previously reported patients are summarized in Table I. The clinical hallmarks include postnatal growth deficiency, thoracic hypoplasia, and retinal abnormalities. Equally affected siblings of opposite gender and the presence of consanguinity in some parents are strongly suggestive of an autosomal recessive pattern of inheritance.

Although birth length is in the normal range, short stature with rhizomelic limb shortening becomes apparent during childhood. Short stature is mild to moderate during childhood; however, growth failure is progressive, and final height may be less than −5 SD. Progressive shortening of the trunk over time results in the ultimately short-trunk body proportion. Thoracic hypoplasia with mild to moderate respiratory distress in the neonatal period is apparent in some cases, while it may be asymptomatic in others. The narrow thorax occasionally gives rise to Harrison grooves and susceptibility to airway infection in infancy and early childhood. Laryngotracheomalacia may contribute to the respiratory problems.

RP or pigmentary retinal degeneration is detectable during childhood and retinal changes may even be observed in the neonatal period. Electroretinography reveals cone-rod dystrophy [Isidor et al., 2010]. Secondary optic atrophy may ensue, and one child (Patient 5) presented cataracts that might be secondary to RP [Jackson et al., 2001]. The prognosis for vision is unfavorable.

As discussed by Isidor et al. [2010], the differential diagnosis includes Shwachman-Bodian-Diamond syndrome (OMIM 260400), Jeune asphyxiating thoracic dysplasia (OMIM 208500), Saldino-Mainzer syndrome (OMIM 266920), Dyggve-Melchior-Clausen (DMC) dysplasia (OMIM 223800), and SMD with cone-rod dystrophy (OMIM 608940). Shwachman-Diamond syndrome causes thoracic hypoplasia and metaphyseal dysplasia most conspicuously in the proximal femora. However, Shwachman-Bodian-Diamond syndrome, unlike axial SMD, is associated with neutropenia and pancreatic exocrine dysfunction but not retinal and spondylar changes. Both Jeune asphyxiating thoracic dysplasia and Saldino-Mainzer syndrome manifest thoracic hypoplasia and retinopathy. Nevertheless, progressive nephropathy and brachydactyly are seen in these disorders and are conspicuously absent in axial SMD. Lacy ilia and spondylar dysplasia in axial SMD may raise a suspicion of DMC. However, DMC shows more severe platyspondyly and epimetaphyseal dysplasia but not retinal changes. SMD with cone-rod dystrophy is a recently identified skeletal dysplasia associated with retinal cone-rod dystrophy. The clinical and radiological pattern in SMD with cone rod dystrophy is similar to that of axial SMD. However, there are clinical and radiological differences between both disorders. Visual impairment is milder in SMD with cone rod dystrophy. Affected individuals do not show complete loss of visual acuity. On the other hand, the skeletal changes of SMD with cone rod dystrophy are much more severe than those in axial SMD. Generalized metaphyseal dysplasia and more severe platyspondyly in SMD with cone rod dystrophy contrast with metaphyseal dysplasia confined to the juxtatruncal bones and mild platyspondyly in axial SMD.

In the neonatal period, axial SMD should be differentiated from SMD Sedaghatian type (OMIM 250220), a perinatally lethal osteochondrodysplasia comprising minor facial, cardiac and cerebral anomalies [Elçioglu and Hall, 1998]. Unlike axial SMD, SMD Sedaghatian type manifests overt metaphyseal dysplasia and lacy ilia in the neonatal period.

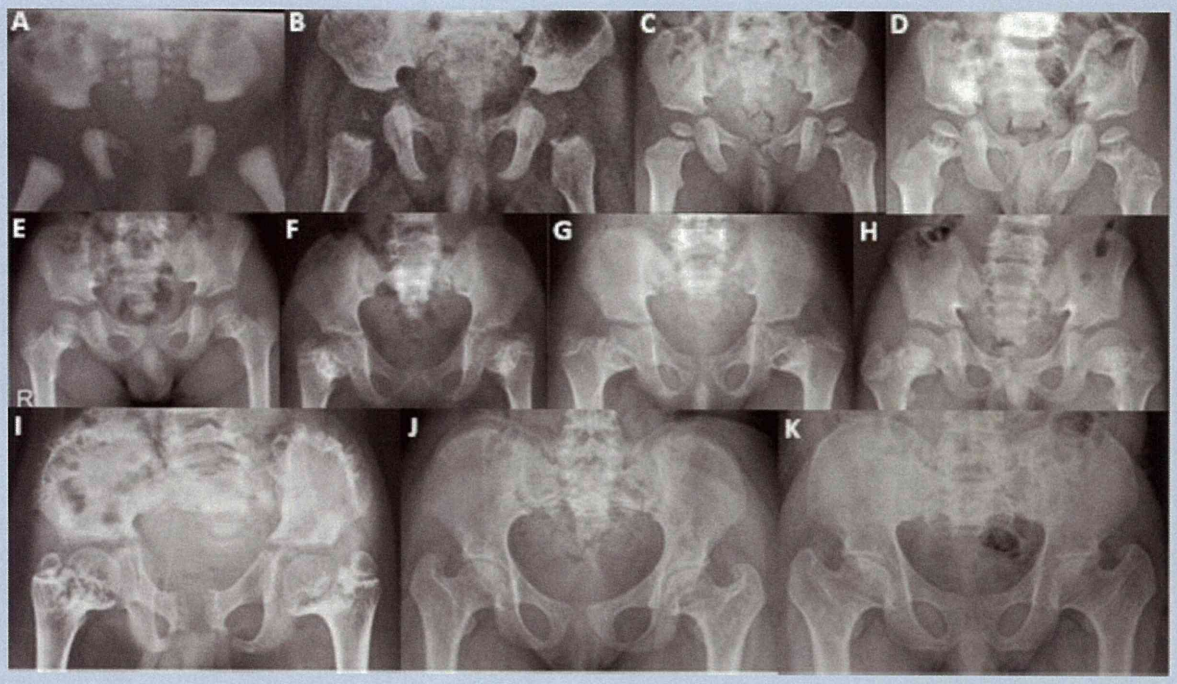

FIG. 5. Radiographs of pelvis. A: Patient 1 at 2 days. The ilia are somewhat hypoplastic but lacy ilia are not evident. B: Patient 1 at age 6 months. The iliac crests are somewhat irregular. C: Patient 2 at age $1^{4/12}$ years. The iliac crests and proximal femoral metaphyses are irregular. D: Patient 3 at age 4 years, (E) Patient 4 at age 5 years. Lacy ilia and metaphyseal irregularities of the proximal femora are apparent. F: Patient 6 at age 8 years, (G) Patient 7 at age 10 years, (H) Patient 4 at age 10 years, (I) Patient 5 at age 12 years. Proximal femoral metaphyseal irregularities with coxa vara are conspicuous in all patients. Lacy ilia are varied among the patients. J: Patient 6 at age 15 years, (K) Patient 7 at age 23 years. Lacy ilia and metaphyseal irregularities already diminish, but coxa vara is persistent.

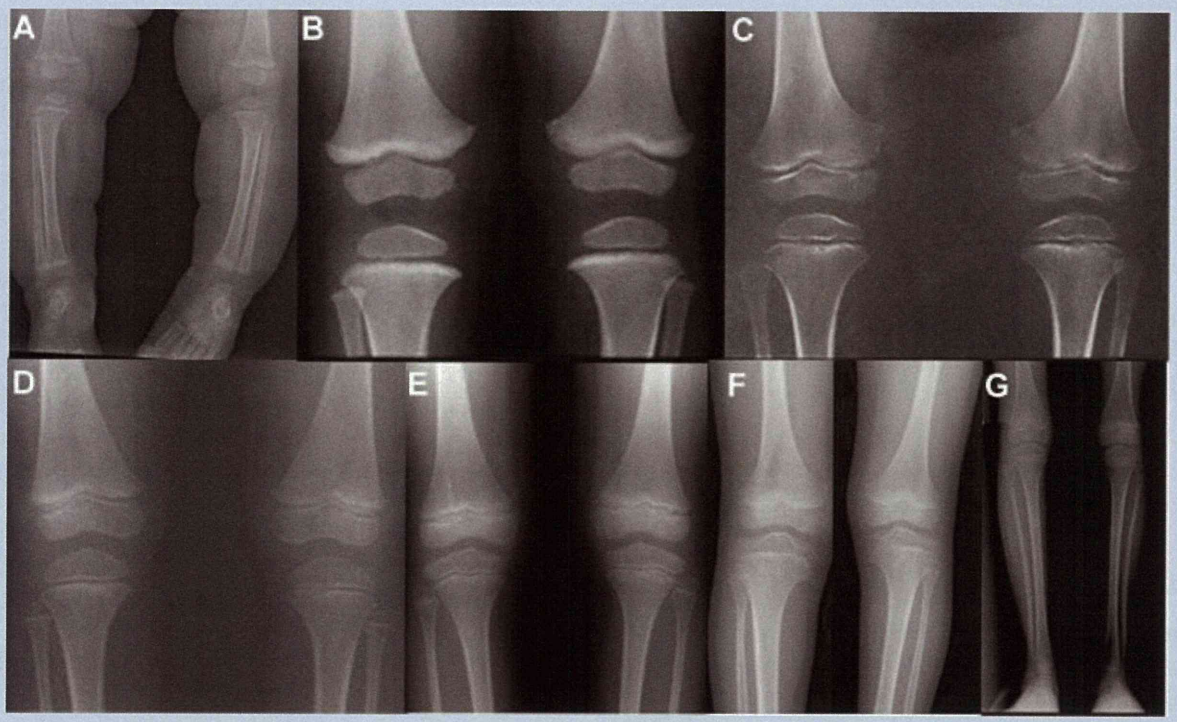

FIG. 6. Radiographs of lower limbs. A: Patient 1 at age 6 months, (B) Patient 2 at age $1^{4/12}$ years, (C) Patient 3 at age 4 years, (D) Patient 6 at age 8 years, (E) Patient 7 at age 10 years, (F) Patient 4 at 10 years, (G) Patient 5 at 12 years. Metaphyseal changes are absent or very mild in the knee but the knee epiphyses are slightly flattened, notably in (B) and (C).

TABLE I. Clinical Characteristics of Patients With Axial SMD

	Present patients							Ehara et al. [1997]	Isidor et al. [2010]		Megarbane et al. [2004]
Patient	**1**	**2**	**3**	**4**	**5**	**6[a]**	**7[a]**	**Case1**	**Patient 1**	**Patient 2**	**Single case**
Race	Japanese	Saudi Arabian	Saudi Arabian	Korean	Japanese	Korean	Korean	Japanese	NA	NA	Lebanese
Sex	Female	Female	Male	Male	Male	Female	Male	Female	Male	Male	Female
Age at last visit (yrs)	0.9	4.5	7	10	12	15	23	5	14	15	4
Family history	Sporadic	Sib	Sib	Sporadic	Sporadic	Sib	Sib	Sporadic	Sporadic	Sporadic	Sporadic
Short stature	−3.4 SD	−4.0 SD	−5.5 SD	−2.0 SD	−6.2 SD	−5.1 SD	−4.7 SD	−3.6 SD	−3.2 SD	−3.6 SD	<3% tile
Small thorax	+	+	+	+	+	+	+	+	+	+	−
Short trunk	−	−	−	+	+	+	+	−	NA	NA	NA
Rhizomelic shortness	+	+	+	+	+	+	+	+	+	+	+
Respiratory disturbance at birth	+	NA	NA	NA	+	NA	NA	−	−	−	NA
Respiratory infection in childhood	NA	NA	NA	NA	+	+	+	+	NA	NA	NA
RP/optic atrophy	+	+	+	+	+	+	+	+	+	+	+
Age of Dx of RP (years)	0	1	0.9	6[b]	0.1	3	8[c]	0.1	5	6.5	3
Scoliosis	−	−	−	+	+	−	−	−	−	−	−

NA, not available; RP, retinitis pigmentosa.

[a]Follow-up study of cases previously described as Case 3 and 2, respectively by Ehara et al. [1997].
[b]Impaired visual acuity was noticed at 5 years of age.
[c]Impaired visual acuity was noticed at 6 months of age.

The molecular basis of axial SMD remains elusive; however, homozygosity mapping and whole genome sequencing techniques should elucidate the disease-causing gene in the near future. Further case reports, sample registration, and investigations will be invaluable in order to thoroughly understand this entity.

ACKNOWLEDGMENTS

This work was in part supported by Research on Child Health and Development (20-S-3) and Ministry of Health, Labor and Welfare of Japan (Measures for Intractable Diseases 046 in 2010).

REFERENCES

Ehara S, Kim OH, Maisawa S, Takasago Y, Nishimura G. 1997. Axial spondylometaphyseal dysplasia. Eur J Pediatr 156:627–630.

Elçioglu N, Hall CM. 1998. Spondylometaphyseal dysplasia-Sedaghatian type. Am J Med Genet A 76:410–414.

Isidor B, Baron S, Khau van Kien P, Bertrand AM, David A, Le Merrer M. 2010. Axial spondylometaphyseal dysplasia: Confirmation and further delineation of a new SMD with retinal dystrophy. Am J Med Genet Part A 152A:1550–1554.

Jackson H, Garway-Heath D, Rosen P, Bird AC, Tuft SJ. 2001. Outcome of cataract surgery in patients with retinitis pigmentosa. Br J Ophthalmol 85:936–938.

Megarbane A, Melick N, Daou L. 2004. A newly recognized skeletal dysplasia with rhizomelic limbs and retinitis pigmentosa. Am J Med Genet Part A 130A:176–180.

Nishimura G, Dai J, Lausch E, Unger S, Megarbane A, Kitoh H, Kim OH, Cho TJ, Bedeschi F, Benedicenti F, Mendoza-Londono R, Silengo M, Schmidt-Rimpler M, Spranger J, Zabel B, Ikegawa S, Superti-Furga A. 2010. Spondylo-epiphyseal dysplasia, Maroteaux type (pseudo-Morquio syndrome type 2), and parastremmatic dysplasia are caused by TRPV4 mutations. Am J Med Genet Part A 152A:1443–1449.

Sousa SB, Russell-Eggitt I, Hall C, Hall BD, Hennekam RC. 2008. Further delineation of spondylometaphyseal dysplasia with cone-rod dystrophy. Am J Med Genet Part A 146A:3186–3194.

Turell M, Morrison S, Traboulsi EI. 2010. Spondylometaphyseal dysplasia with cone-rod dystrophy. Ophthalmic Genet 31:12–17.

Warman M, Cormier-Daire V, Hall C, Krakow D, Lachman R, LeMerrer M, Mortier G, Mundlos S, Nishimura G, Rimoin DL, Robertson S, Savarirayan R, Sillence D, Spranger J, Unger S, Superti-Furga A. 2011. Nosology and classification of genetic skeletal disorders: 2010 Revision. Am J Med Genet Part A 155A:943–968.

Wirth T. 2008. Spondyloepiphyseal and metaphyseal dysplasia. Orthopade 37:8–16.

Jpn J Ophthalmol (2011) 55:264–267
DOI 10.1007/s10384-011-0020-8

CLINICAL INVESTIGATION

Nishida's procedure combined with medial rectus recession for large-angle esotropia in Duane syndrome

Michiko Tanaka · Sachiko Nishina · Shigeko Ogonuki · Shouko Akaike · Noriyuki Azuma

Received: 18 August 2010 / Accepted: 12 December 2010 / Published online: 11 May 2011

Abstract
Background Two patients presented large-angle esotropia due to unilatelal Duane syndrome type I.
Cases We report the course of a simple muscle transposition procedure (the Nishida procedure) with medial rectus muscle recession for large-angle esotropia in two cases of unilateral Duane syndrome type I.
Observations Case 1: A 5-year-old boy had Duane syndrome type I OS. He had esotropia of 40 prism diopters, and the left eye could not abduct to the midline. Postoperatively, his esotropia decreased to 6 prism diopters and the abduction improved to 45°. Case 2: A 5-year-old girl had Duane syndrome type I OS with a marked facial turn. She had esotropia of 40 prism diopters in primary position, and the left eye could not abduct to midline. Postoperatively, the facial turn resolved, the esotropia decreased to 8 prism diopters, and the abduction improved to 30°.
Conclusion This procedure improves large-angle esotropia and abduction deficits in unilateral Duane syndrome type I.

Keywords Duane syndrome · Esotropia · Surgery · Nishida's procedure

M. Tanaka · S. Nishina (✉) · S. Ogonuki · S. Akaike · N. Azuma
Division of Ophthalmology,
National Center for Child Health and Development,
2-10-1 Okura, Setagaya-ku, Tokyo 157-8535, Japan
e-mail: nishina-s@ncchd.go.jp

Introduction

Duane syndrome type I is a common congenital ocular motility disorder, characterized by either orthophoria or esotropia with marked limitation of abduction, mild limitation of adduction with retraction, and pseudoptosis. Various surgical procedures have been advocated to improve the esotropia, facial turn, and abduction deficits. The two major approaches are medial rectus muscle recession and vertical rectus muscle transposition; however, neither procedure can correct the large-angle esotropia in unilateral Duane syndrome type I without complications.

We used a new simple muscle transposition procedure (the Nishida procedure) with medial rectus recession for large-angle esotropia in two cases of unilateral Duane syndrome type I. This procedure includes vertical rectus muscle transposition without tenotomy or muscle splitting [1].

Case report

Case 1

A 5-year-old boy had Duane syndrome type I OS. He had left esotropia of 40 prism diopters (PD) in primary position and mild amblyopia OS. Ductions of the affected eye were evaluated using a six-point scale [2, 3], in which 0 indicates full movement, −1 restriction to 45° of abduction, −2 limited movement to 30°, −3 limited movement to 15°, −4 inability to move the eye past the midline, and −5 inability to rotate the eye to midline. The left eye could not abduct to the midline (−5) (Fig. 1a, b). He did not have any other ocular or systemic abnormalities. Magnetic resonance imaging (MRI) did not show brain or extraocular muscle

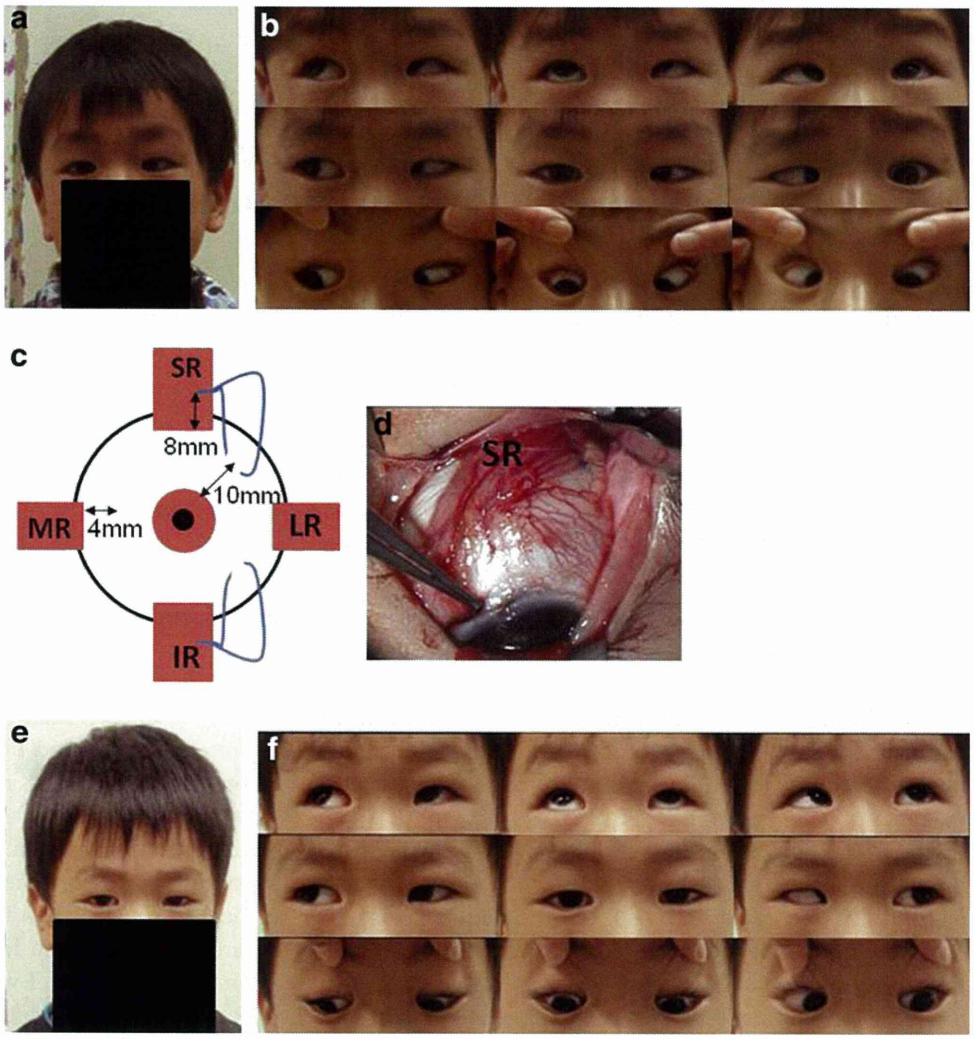

Fig. 1 Case 1. **a** Preoperative head position and left esotropia of 40 prism diopters. **b** A nine-gaze photograph shows a significant abduction deficit (−5) OS and narrowing of the left palpebral fissure on right gaze preoperatively. **c** Nishida's procedure combined with medial rectus recession. The 6-0 polypropylene sutures are passed through each vertical rectus at a distance of 8 mm behind their insertions and passed through each sclera at a distance of 10 mm behind the limbus. *SR* superior rectus, *IR* inferior rectus, *LR* lateral rectus, *MR* medial rectus. **d** The superior rectus muscle (*SR*) is transposed without tenotomy or muscle splitting, and anchored onto the superotemporal sclera. **e** A normal head position and mild esotropia of 6 prism diopters postoperatively. **f** A nine-gaze photograph shows marked improvement of the left abduction to −1 and a −1 point adduction deficit postoperatively

abnormalities. The visual acuity (VA) OS improved to 20/20 with amblyopia treatment; however, because of the residual large-angle esotropia of 40 PD, the patient often compensated with left facial turn and right head tilt for fusion. He demonstrated sensory fusion with major amblyoscope, but stereopsis was not detected with the Titmus stereo test.

He underwent the Nishida procedure with 4-mm of medial rectus recession OS. Because the left medial rectus muscle was tight with positive forced duction, tenotomy of the medial rectus muscle was performed initially, following that the vertical recti were explored, and 6-0 polypropylene sutures were passed through the temporal margins and tied 8 mm behind their insertion points. An identical suture was passed through the sclera 10 mm behind the superotemporal and inferotemporal limbus, and each vertical rectus muscle was transposed either superotemporally or inferotemporally and anchored on the sclera (Fig. 1c, d). Finally, the medial rectus muscle was anchored 4 mm behind its insertion point.

Postoperatively, the esotropia decreased to 6 PD, and the abnormal head posture resolved throughout the 1-year follow-up period. The binocular function remained unchanged. Abduction significantly improved from −5 to −1. A −1 point adduction deficit developed in the left eye, but no vertical deviation developed (Fig. 1e, f).

Case 2

A 5-year-old girl had Duane syndrome type I OS with marked left facial turn. She had left esotropia of 40 prism diopters in primary position and mild amblyopia OS. The left eye could not abduct to midline (−5). She did not have any other abnormalities. MRI did not show brain or extraocular muscle abnormalities. The VA OS improved to 20/25 with amblyopia treatment; however, there was residual large-angle esotropia of 40 PD and left facial turn to achieve fusion (Fig. 2a, b). She demonstrated sensory fusion with major amblyoscope, but stereopsis was not

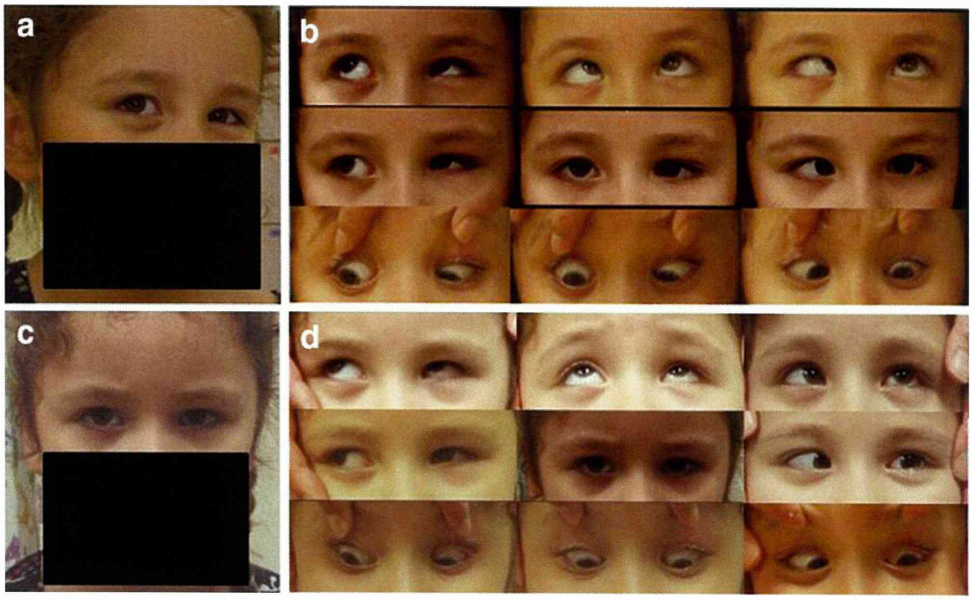

Fig. 2 Case 2. **a** Substantial preoperative left facial turn. **b** A nine-gaze photograph shows left esotropia of 40 prism diopters, a substantial abduction deficit (−5) OS and narrowing of the left palpebral fissure on right gaze preoperatively. **c** A normal head position and slight esotropia of 8 prism diopters postoperatively. **d** A nine-gaze photograph shows improvement of the left abduction to −2 and a −1 adduction deficit postoperatively

detected with the Titmus stereo test. The same procedure as described in case 1 was performed on her left eye.

Postoperatively, the esotropia decreased to 8 PD and the abnormal head position resolved. The abduction improved from −5 to −2. A −1 point adduction deficit developed in her left eye, but vertical deviation did not develop (Fig. 2c, d).

Discussion

Surgical procedures such as medial rectus muscle recession and vertical rectus muscle transposition have proved inadequate to correct large-angle esotropia in patients with unilateral Duane syndrome type I [2–8]. Medial rectus recession is the standard procedure to correct an average of 20–25 prism diopters of esotropia, straighten the ocular position, and resolve the aberrant head position; however, it cannot improve abducens excursion. Four to 6% of patients develop exotropia postoperatively [2, 4], and excessive recession exceeding 6 mm may cause a severe adduction deficit [5]. Medial rectus recession was necessary in the present cases to treat the tight medial rectus muscles, but excessive recession for large-angle esotropia should be avoided. Vertical rectus muscle transposition can correct a maximum of 30 prism diopters of esotropia and improve abducens excursion [3, 6–8]; however, the surgical effect seems unpredictable, and 8.5% of patients may develop a vertical deviation postoperatively [9]. The procedure also has the risk of anterior segment ischemia in patients with systemic complications.

In the current cases, using the Nishida procedure, including vertical rectus muscle transposition without tenotomy or muscle splitting, we simultaneously performed vertical rectus muscle transposition and medial rectus recession, and successfully corrected large-angle esotropia exceeding 30 prism diopters and a severe abduction deficit. No vertical deviation developed, and a minimal adduction deficit was present as a result of the procedure. Cases need to be observed to confirm the long-term stability of alignment, and further study of this procedure will be needed to clarify the risk of overcorrection and vertical deviation induced. A simple medial rectus recession is generally recommended as an effective procedure with minimal complications for small-angle esotropia in most patients with Duane syndrome type I, and this procedure may be necessary for a few severe cases. Although the number of cases here was small, this new procedure may effectively and safely improve large-angle esotropia and abduction deficits in patients with unilateral Duane syndrome type I.

Acknowledgments The authors thank Yasuhiro Nishida, MD, PhD, for his technical advice.

Conflict of interest The authors have no proprietary interest in any aspect of this report.

References

1. Nishida Y, Hayashi O, Oda S, Kakinoki M, Myake T, Inoki Y, et al. A simple muscle transposition procedure for abducens palsy without tenotomy or splitting muscles. Jpn J Ophthalmol. 2005;49:179–80.
2. Barbe ME, Scott WE, Kutschke PJ. A simplified approach to the treatment of Duane's syndrome. Br J Ophthalmol. 2004;88:131–8.
3. Britt MT, Velez FG, Velez G, Rosenbaum AL. Vertical rectus muscle transposition for bilateral Duane syndrome. J AAPOS. 2005;9:416–21.
4. Kubota N, Takahashi H, Hayashi T, Sakaue T, Maruo T. Outcome of surgery in 124 cases of Duane's Retraction Syndrome (DRS)

treated by intraoperatively graduated recession of the medial rectus for esotropic DRS, and of the lateral rectus for exotropic DRS. Binocul Vis Strabismus Q. 2001;16:15–22.
5. Nelson LB. Severe adduction deficiency following a large medial rectus recession in Duane's retraction syndrome. Arch Ophthalmol. 1986;104:859–62.
6. Foster RS. Vertical muscle transposition augmented with lateral fixation. J AAPOS. 1997;1:20–30.
7. Gobin MH. Surgical management of Duane's syndrome. Br J Ophthalmol. 1974;58:301–6.
8. Molarte AB, Rosenbaum AL. Vertical rectus muscle transposition surgery for Duane's syndrome. J Pediatr Ophthalmol Strabismus. 1990;27:171–7.
9. Ruth AL, Velez FG, Rosenbaum AL. Management of vertical deviations after vertical rectus transposition surgery. J AAPOS. 2009;13:16–9.

Fluorescein Staining of the Vitreous During Vitrectomy for Retinopathy of Prematurity

Vitreous staining using triamcinolone acetonide[1] or fluorescein[2] generally has been used even in children[3] to visualize the preretinal membrane and vitreous during vitrectomy.

During the surgery for retinopathy of prematurity (ROP), careful segmentation and extensive vitreous cutting are required around the base of tractional retinal detachments, vitreous base, and fibrovascular tissue.[4] Removal of the formed vitreous around the fibrovascular tissue and the vitreous base is a key factor for a successful surgery.[4] To remove the vitreous safely, good intraoperative visualization of the vitreous is essential.

In the current study, we included cases of aggressive posterior ROP in which wide-field vitrectomies are necessary to evaluate the staining of the entire vitreous. We describe a technique for staining the vitreous with fluorescein and compared it with staining using triamcinolone in these patients with ROP.

Patients and Methods

This study included 45 consecutive eyes with Stage 4A aggressive posterior ROP, which required vitrectomies with lensectomies to be performed in 30 babies (mean age, 24 weeks; range, 22–30 weeks); no infant had undergone a previous surgery. The same surgeon (N.A.) performed all the surgeries in our hospital between June 2005 and May 2008. All aspects of this study were approved by the institutional ethics committee, and the parents of the patients provided informed consent before the infants were enrolled in the study. The mean follow-up duration in the triamcinolone group was 32 months (range, 15–38 months), and in the fluorescein group, the mean follow-up duration was 28 months (range, 12–32 months).

From the Department of Ophthalmology, National Center for Child Health and Development, Tokyo, Japan.

The authors have no financial interest in any aspect of this report.

Reprint requests: Yuri Kobayashi, MD, Noriyuki Azuma, MD, PhD, 2-10-1 Okura Setagaya-ku, Tokyo, 157-8535, Japan; e-mail: azuma-n@ncchd.go.jp

The demographics of the study group are shown in Table 1. There was no difference in the severity of ROP between the two groups. All patients underwent a 3-port 25-gauge vitrectomy using a small contact lens designed for premature eyes. The other instruments, including infusion pipes, cannulas, and light pipes, were used as in the conventional 25-gauge system. We previously described the procedures of early vitreous surgery for ROP.[4,5] In 27 eyes of 18 patients, sodium intravenous fluorescein (0.1 mL/kg) was injected preoperatively for fluorescein angiography and to visualize the vitreous gel intraoperatively. The intervals between fluorescein angiography and vitrectomy ranged from 10 minutes to 20 minutes. When both eyes required surgery, the mean time to surgery in the other eye was approximately 50 minutes. In the other study group, 0.2 mL of triamcinolone was injected repeatedly into the vitreous cavity in 18 eyes of 12 patients to visualize the residual vitreous after lensectomy and core vitrectomy. The authors evaluated the staining pattern of the vitreous, the postoperative results, and any complications. Analyses were performed, and categorical differences were compared using Fisher's test. All P values were 2-sided, and $P < 0.05$ was considered statistically significant. Analyses were conducted using GraphPad Prism5.0 statistical software (GraphPad Prism Software Institute, La Jolla, CA).

Results

Injections of triamcinolone were required three to five times during the surgery because we could not achieve full visualization of the distance between the residual vitreous and the retinal surface; triamcinolone was only on the cut surface of the vitreous, and the vitreous gel beneath remained transparent. In contrast, fluorescein dye produced homogenous and full-thickness staining (Figure 1), especially around the fibrovascular tissue and the vitreous base (Figure 2), which was sufficiently stained green but remained transparent.

When fluorescein was used, an iatrogenic break occurred in 1 eye (3.7%) as a result of an unstable 25-gauge infusion cannula. The break was repaired by